MODEL TESTING OF FOUNDATIONS FOR OFFSHORE WIND TURBINES

by

Felipe Alberto Villalobos Jara

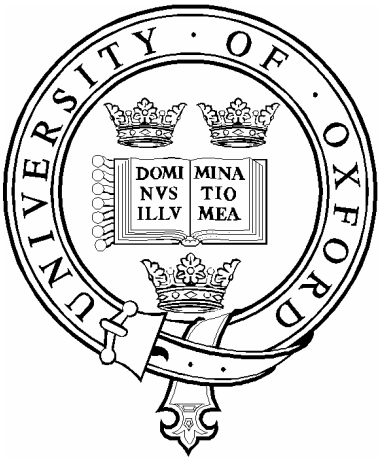

A thesis submitted for the degree of
Doctor of Philosophy
at the University of Oxford

Keble College, Michaelmas Term 2006

ABSTRACT

Model testing of foundations for offshore wind turbines

A thesis submitted for the degree of Doctor of Philosophy

Felipe Alberto Villalobos Jara
Keble College, Oxford
Michaelmas Term 2006

Suction caissons are a new foundation option for offshore wind turbines. This thesis is focussed on the behaviour of suction caisson foundations in sand and in clay during installation, and under subsequent vertical and combined moment-lateral loadings. The research is based on extensive experimental work carried out using model scaled caissons. The analysis of the results allowed the determination of parameters for hyperplasticity models. Model caissons were vertically loaded in loose and dense sands to study in service states and plastic behaviour. Bearing capacity increased with the length of the caisson skirt. The bearing capacity formulation showed that the angle of friction mobilised was close to the critical state value for loose sands and close to those of peak values due to dilation for dense sands. The vertical load increased, though at a lower rate than during initial penetration, after large plastic displacements occurred. A hardening law formulation including this observed behaviour is suggested. In sand the installation of caissons by suction showed a drastic reduction in the net vertical load required to penetrate the caisson into the ground compared with that required to install caissons by pushing. This occurred due to the hydraulic gradients created by the suction. The theoretical formulations of the yield surface and flow rule were calibrated from the results of moment loading tests under low constant vertical loads. The fact that caissons exhibit moment capacity under tension loads was considered in the yield surface formulation. Results from symmetric and non symmetric cyclic moment loading tests showed that Masing's rules were obeyed. Fully drained conditions, partially drained and undrained conditions were studied. Caisson rotation velocities scaled in the laboratory to represent those in the field induced undrained response for relevant periods of wave loading, a wide range of seabed permeabilities and prototype caisson dimensions. Under undrained conditions and low constant vertical loads the moment capacity of suction caissons was very small. Under partially drained conditions the moment capacity decreased with the increase of excess pore pressure. In clay, vertical cyclic loading around a mean vertical load of zero showed that in the short term the negative excess pore pressures generated during suction installation reduced vertical displacements. The yield surface and the flow rule were determined from moment swipe and constant vertical load tests. The moment capacity was found to depend on the ratio between the preload V_o and the ultimate bearing capacity V_u. Gapping response was observed during cyclic moment loading tests, but starting at smaller normalised rotations than in the field. The hysteresis loop shape obtained during gapping cannot be reproduced by means of the Masing's rules.

ACKNOWLEDGEMENTS

I would like to thank Professor Houlsby for offering me the Research Assistance post, without which my research would not have been possible. I am also in debt to Professor Houlsby for his patience in reading my thesis and for giving me useful comments. I am also grateful to Dr Byrne for allowing me the use of the computer programs to control the VMH loading rig. Similarly, I would like to thank Dr Byrne for reading my thesis and for giving me valuable contributions. I would also express my gratitude to Professor Sills for allowing me the use of equipment of the environmental soil mechanics laboratory and encouraging me during my research.

I am grateful to the Department of Trade and Industry and the Engineering and Physical Sciences Research Council for funding this research as part of the larger DTI Future Energy Solutions project. I would like to acknowledge engineers in SLP Engineering Ltd, Shell Renewables Ldt, Fugro Ldt, Garrad Hassan, and HR Wallingford for interesting discussions in meetings as part of the DTI research project.

I want to thank to the laboratory technicians Bob, Chris and Clive for their help. I am grateful to the researchers in Room 11 and in the soil mechanics laboratory Kaori Kuribayashi, Gwyn Lintern, Gert Bartholomeeussen, John Pickhaver, Nick Melin, Giang Nguyen, Suched Likitlersuang, KK, Jackie Sim, Paul Bonnet, Mattia Rovere, Mobin Ojaghi, Anthony Comer, Ed Hazell and Phil Price for their camaraderie reflected in chats and activities in and out of work. Many thanks to Peter for interesting conversations about cultures, art and artists.

I shared the days in Oxford with many new friends. Salvador Venegas, Dolores Sanchez, Matthew Niblett, Berny Sèbe and Tom Brennan from Keble College. Richard Campbell, David Cocks, Misha and Rebecca from the Walking Club. Mario, Serguei and Rosana from the Mexican Society. Jeff, Olivia, Ross, Mikhail, Thomas and Yoshi from Merton College. Oliver Bleskie, Sanjeev Krishna, Kulviar and Bobby Jones from Magdalen College. And my friends Josh, Justin, Simon and Victor for good football games.

I want to especially thank my *petite amie* Claire for accompanying me along this journey. I also met new compatriot friends Yerko, Nicole, Javier, Catalina, Francisco, Meredith, Jaime and Jo, with whom I enjoyed delicious meals and wines as well as yaps. I met friends Matt, Fabiola and Phil in London, Ingo in Hannover, and Miguel Pereira in Hamburg with whom I had wonderful moments. I want to express my gratitude to Professor Verdugo who showed constant interest in my research as well as Mr Barrera. My friends and colleagues Pato and Diego have always been in contact with good sense of humour. Infinite thankfulness to my family, especially my cousin Hugo and my mother who send me more email 'letters' than anybody else.

LIST OF SYMBOLS

A	caisson lid cross area
A	strip flat footing area $= BL$
A	shear modulus material constant
B	strip footing width
B_c	cohesion component of bearing capacity
B_q	surcharge component of bearing capacity
B_γ	weight component of bearing capacity
C	settlement service state formulation constant
C_c	coefficient of curvature
C_D	drag coefficient
C_M	inertia coefficient
C_s	shape factor
C_t	thixotropy strength ratio
C_u	coefficient of uniformity
D	depth
D_f	fluid depth
D_s	grain size
D_{10}	average grain diameter of the 10% passing
DOF	degree of freedom
E	Young's modulus
F	dimensionless flow factor
F	frictional force
F_D	drag force
F_M	inertia force
F_T	thrust force
G	shear modulus
G_s	soil specific gravity
H	horizontal load
H_s	significant wave height
K	absolute permeability
K	lateral earth pressure coefficient
K	$K_P - K_A$
K_A, K_P	Krynine active and passive pressure coefficients
K_i	foundation stiffness $i = v, m, h$
K_i	theoretical foundation stiffness coefficients for $i = V, M, MH, H$
L	wave length
L	strip footing length
L	caisson skirt length
$L/2R$	caisson aspect ratio
LL	liquid limit
LRP	load reference point
$M/2R$	moment load
$M/2RH$	load ratio
M_o	constrained modulus
N_c	cohesion bearing capacity factor
N_q	surcharge bearing capacity factor
N_F	number of flow channels
N_H	number of pressure drops
N_γ	weight bearing capacity factor

NC	normally consolidated
OC	over consolidated
OCR	overconsolidation ratio
PL	plastic limit
PPT	pore pressure transducer
Q	soil mineralogy parameter
Q	deviatoric load
R	radius
$2R$	diameter
$2R\theta$	rotational displacement
R_d	relative density
R_n	normalised roughness
R_{max}	maximum roughness
S	suction force
S_t	sensitivity
T	wave period
T	total shear vane torque
T	temperature
T_v	dimensionless time factor during consolidation
V'	buoyant or submerged vertical load
V_c	contact vertical load
V_m	mean vertical load
V_o	maximum vertical load experienced by the foundation
V_t	drained tension load
V_u	ultimate bearing capacity load
W	submerged weight of the caisson, soil plug and water column
Z	stress distribution function

a	load-settlement curve initial slope
a	pore pressure factor
a	factor of depth below the caisson
a_1	pore pressure factor for $k_f = 1$
$a_{V_1}, a_{V_2}, a_M, a_H$	association factors
b	peak vertical load parameter
c	cohesion
c	post-bearing capacity failure parameter
c_D	drag coefficient
c_M	inertia coefficient
c_T	thrust coefficient
c_v, c_h	coefficient of vertical and horizontal consolidation
c_0, c_1, c_2	pressure factor equation parameters
d	vane diameter
d	distance between LRP and another point of load application
d	dissipation function
d_q, d_γ	depth factors
d_w	water depth
e	eccentricity
f_o, f_i	outside and inside soil arching variation
f_p	post peak load parameter

g	acceleration of gravity
h	vane length
h	caisson penetration
$\dot{h}$	caisson penetration velocity
h_c	contact penetration
h_f	head diference
h_i	yield surface intersection with horizontal load axis
h_o	horizontal load dimension of yield surface
h_{om}	horizontal load dimension of yield surface at the metacentre
h_p	caisson self-weight penetration
h_{pe}	estimated caisson self-weight penetration
h_t	penetration at maximum tension load
i	hydraulic gradient
i_c	critical hydraulic gradient
k	coefficient of permeability
k_a, k_p	Rankine active and passive lateral earth pressure coefficients
k_f	permeability ratio
k_i	theoretical dimensionless stiffness coefficients for $i = v, m, mh, h$
m	constant of soil arching extension
m_i	yield surface intersection with moment load axis
m_o	moment load dimension of yield surface
m_{om}	moment load dimension of yield surface at the metacentre
n	exponent of shear modulus function
p'	mean effective stress
p_a	atmospheric pressure
p_{cav}	cavitation pressure
q	steady flow rate
q	radial displacement
$\dot{q}$	radial displacement increment
q_c	cone resistance
s	spacing between caissons in a multiple caisson foundation
s	suction
s_u	undrained shear strength
t	time
t	caisson skirt wall thickness
$t/2R$	thickness ratio
t_o	yield surface tension parameter
t_p	time of full caisson penetration
t_s	time of caisson penetration under suction assistance
u	horizontal displacement
u'	excess pore pressure
v	caisson velocity
v_n	non-dimensional footing velocity
v_1	wind far upstream velocity

w	water content
w	vertical displacement
w_s	vertical displacement at lowest softening load
w_t	total vertical displacement
y	yield surface
z_m	depth of the metacentre
Λ	critical state parameter
Θ	vane rotation
Ω	rotor speed
α	adhesion factor
α	maximum yield surface dimension
α_i	internal variable and plastic displacement for $i = V, M, H$
$\dot{\alpha_i}$	plastic displacement increment for $i = V, M, H, Q$
β_1, β_2	yield surface curvature parameters
γ	soil unit weight
γ'	buoyant soil unit weight
γ_d	dry soil unit weight
γ_f	fluid unit weight
γ_w	water unit weight
δ	interface angle of friction
θ	spiral fan angle
θ	soil arching angle
θ	caisson rotation
κ	unloading-reloading slope in $\upsilon - lnp'$ plane
λ	blade tip speed ratio
λ	slope of normal compression line in $\upsilon - lnp'$ plane
λ	multiplier in the flow rule formulation
μ_d	dynamic viscosity
μ_k	kinematic viscosity
ν	Poisson's ratio
ρ	shear strength gradient
ρ_a	air density
ρ_f	fluid density
ρ_w	water density
σ'_{ij}	stress tensor
σ'_1, σ'_3	principal stresses
σ'_n	normal stress
σ'_r	radial stress
$\sigma'_{v_{seepage}}$	seepage vertical stress
σ'_v	vertical effective stress
$\Delta\sigma'_v$	consolidation vertical stress increment
σ'_{vo}	maximum vertical effective stress during consolidation
σ'_{vi}	vertical effective stress once $\Delta\sigma'_v$ is removed after swelling
τ	shear stress
υ	specific volume
υ_{cs}	critical state specific volume

ϕ'	angle of friction
ϕ'_{cs}	critical state angle of friction
ϕ'_{mob}	mobilised angle of friction
ϕ'_{peak}	peak angle of friction
χ	dissipative generalised load
$\bar{\chi}$	generalised load
ψ	wave number
ω	angular wave frequency

$crit$	critical
e	elastic
f	final
h	horizontal
i	initial
i	inside
m	mean
max, min	maximum, minimum
mh, hm	coupled
o	outside
p	plastic
v	vertical
y	yield
δ	increment
Δ	variation

Contents

Chapter 1

INTRODUCTION

Abstract

The current renewable energy policy in the UK has motivated this research. This chapter starts describing the beginning and evolution of the now worldwide growing offshore wind energy industry. The particular characteristics of the environmental loads offshore, type of seabed soils and foundations commonly adopted are explained. The type of structure and loading regime establish new conditions from a civil engineering point of view. Suction caissons are introduced as an alternative foundation for offshore wind turbines. Suction caissons are currently an accepted alternative to pile foundations in applications for the oil and gas industry. However, this is not yet the case in applications for offshore wind turbines. A review of previous experimental and theoretical studies of shallow foundations is presented. A new theoretical approach referred to as hyperplasticity allows simpler and rigorous models to be constructed, which are suited for modelling monotonic, and more importantly, cyclic response of shallow foundations. However, little experimental research has been performed to calibrate and validate hyperplastic models. Therefore, experimental research is found to be essential to study the effects of different loading conditions, soil types and caisson geometries on the foundation response, interpreting the results within the hyperplasticity framework. It is concluded that the final objective of this research is to contribute to the design of suction caisson foundations for offshore wind turbines.

1.1 FOUNDATIONS FOR OFFSHORE WIND TURBINES

1.1.1 Motivation for the research project

The need for increased production of clean and sustainable energy in the near future has resulted in a search for alternatives to fossil fuels as sources of energy. Wind energy is one of the most promising options for electricity generation, with optimistic growth forecasts for the near future. The UK Government, in the Renewables Obligations (DTI, 2002), is implementing a renewable energy policy to reduce CO_2 emissions, with the target to supply from renewable sources 10% of the total electricity consumed in 2010, and according to the DTI (2003) 20% in 2020. Currently, seven offshore wind farms are operating along the UK coasts (Table 1.1). As part of the first round of offshore wind farm projects (*ca.* 630 turbines, totalling around 1700 MW) another 10 wind farms will be soon built and another 15 are announced to be built in the next ten years as part of the second round of projects (*ca.* 2000 turbines, totalling around 7100 MW). Given that, it is estimated that offshore wind energy will be capable of providing around 9% of the UK's electricity supply. However, if the 20% of electricity were supplied by offshore wind (using 3.5 MW turbines) another 3200 turbines might be necessary to achieve the remainder 11% target.

Within this context, a large research project was undertaken by an industry-university partnership with the aim of improving current design methods used for placing wind turbines offshore. At the University of Oxford the research has focused on the study of a novel foundation for offshore wind turbines. Information about the work at Oxford can be found in Houlsby and Byrne (2000), Byrne *et al.* (2002), Byrne and Houlsby (2003, 2006) and Villalobos *et al.* (2004b).

The design of foundations is based on a balanced proportion of theories and empiricism. A predominantly empirical approach is suitable when the type of foundation is familiar to

the geotechnical engineer due to previous experience. However, in the presence of a novel type of foundation such an approach may lead to too much risk. To employ a novel foundation in practice with confidence a complete investigation of its response under different likely loading conditions should be undertaken. This is the main motivation behind the work presented in this thesis. The reasons for studying novel foundations such as suction caissons for offshore wind turbines, are explained in sections §1.1.6 and §1.1.7.

1.1.2 The offshore wind energy industry

The use of wind as a source of energy dates from centuries ago. A milestone was reached in the 18^{th} century when around 200000 windmills were rotating in Europe to grind corn or pump water. But in 1888 Charles Brush built the first wind turbine to generate electricity. Improvements in turbine efficiency led to the construction of thousands of *onshore* wind turbines particularly in California in the 1980's and in Germany in early 2000's. Protests by communities about the turbines' visual and noise 'contamination' brought support to the relatively new idea of harnessing the wind energy from *offshore*, where it is also more intense. In fact, Kühn (2002) shows that theoretically there is enough exploitable offshore wind resource to supply completely the electricity consumption in Europe. In 1998 the annual electricity consumption of the EU states was 2500 TWh, which according to Figure 1.1 could be obtained from wind farms located between 30 and 40 km from the shore with water depths between 20 and 30 m.

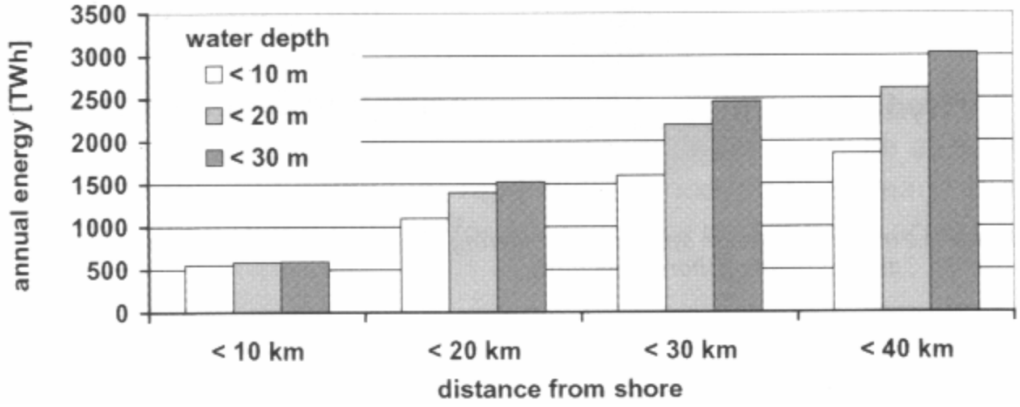

Figure 1.1: Estimated offshore wind energy potential in Europe (taken from Kühn, 2002)

In 1985 a row of 16 wind turbines were founded on an embankment pier in the harbour of

Ebeltoft, Denmark. However, it is considered that Nogersund in the Baltic sea, Sweden, became in 1991 the first operating *offshore* wind turbine. It was erected with a generation capacity of 220 kW, at 250 m from the shore and in 7 m water depth. Also in 1991 the world's first offshore wind farm was constructed at Vindeby, Denmark. Eleven turbines with a capacity of 450 kW each compose the wind farm with turbines resting on gravity base foundations 1.5 km from the shore and between 3 and 5 m water depth. A summary of the existing and about-to-be-completed offshore wind farms is presented in Table 1.1.

Table 1.1: Operating offshore wind farms in the world

Online	Wind Farm	Country	N°	MW	Foundation	do[1], km	wd[2], m
1991	Nogersund	S	1	0.2	mP	0.25	7
1991	Vindeby	DK	11	5	GB	1.5	3-5
1994	Medemblik (Lely)	NL	4	2	MP	0.75	5-10
1995	Tunø Knob	DK	10	5	GB	3-6	3-5
1996	Dronten	NL	19	11.4	MP	0.02	5
1997	Bockstigen	S	5	2.5	MP	3	6
2000	Blyth	UK	2	3.8	MP	0.8	6-11
2001	Middelgrunden	DK	20	40	GB	3	3-6
2001	Uttgrunden	S	7	10.5	MP	8	7-10
2001	Yttre Stengrund	S	5	10	MP	5	6-10
2002	Horns Rev	DK	80	160	MP	14-20	6-14
2003	Samsø	DK	10	23	MP	3.5	15-18
2003	Frederikshavn	DK	4	10.6	MP & SC	0.2	4
2003	Rødsand (Nysted)	DK	72	165	GB	6	6-9.5
2003	North Hoyle	UK	30	60	MP	7-8	10-20
2004	Scroby Sands	UK	30	60	MP	2.3	4-8
2004	Arklow Bank	IRL	7	25.2	MP	12	2-5
2004	Ems-Emden	D	1	4.5	CC	0.04	3
2005	Barrow	UK	30	90	MP	8	15-20
2005	Wilhelmhaven	D	1	4.5	SC	0.55	5
2005	Kentish Flats	UK	30	90	MP	8.5	5
2006	Breitling	D	1	2.5	CC	0.5	2
2006	Egmond	NL	36	108	MP	18	16-22
2007	Beatrice	UK	2	10	mP	25	45
2007	Lillgrund	S	48	110	GB	7	3
2007	Burbo	UK	25	90	MP	10	1-8
		Total:	491	1104			

[1] distance offshore, [2] water depth; GB: gravity base, MP: monopile, mP: multiple piles, SC: suction caisson, CC: concrete cylinder

An estimation per country of the number of turbines and the capacity for the next few years is presented in Table 1.2. By comparison with the current situation there will be an increase by approximately 20 times in the number of turbines, which will generate 40 times more electricity. The future scenario is very promising. Germany and the UK

Table 1.2: Estimated future growing of turbine number and capacity in the world

Country	N°	MW	source
Belgium	60	300	www.offshorewindenergy.org/
China	40	200	*Windpower Monthly*
Denmark	130	400	www.windpower.org/
France	232	700	www.iwr.de/wind/offshore/
Germany	6122	27300	www.iwr.de/wind/offshore/
Ireland	433	1205	www.iwea.com/offshore/
Netherland	96	220	www.iwr.de/wind/offshore/
Polan	100	200	www.iwr.de/wind/offshore/
Spain	170	450	www.iwr.de/wind/offshore/
Sweden	630	2040	www.iwr.de/wind/offshore/
USA	519	1260	www.iwr.de/wind/offshore/
UK	2705	10151	www.bwea.com/
Total:	11237	44376	

are the countries with the most ambitious programmes (see for example the magazines *Windpower Monthly* and *Renewable Energy World* for updated information).

1.1.3 Environmental load of the wind

The wind velocity can be considered useful to harness energy if it is above 3 m/s (light wind), but full production (though varies with device) requires 12 m/s (strong wind). The wind to stop electricity generation is above 25 m/s (storm). The aerodynamic force generated by the wind on a turbine can be assumed proportional to the wind dynamic pressure $\frac{v_1^2 \rho_a}{2}$ multiplied by the rotor swept area πR^2, where v_1 is the far upstream wind speed, ρ_a is the air density, and R is the rotor radius. Then the thrust force is giving by:

$$F_T = \frac{1}{2}\rho_a \pi R^2 v_1^2 c_T(\lambda) \tag{1.1}$$

where the thrust coefficient c_T accounts for the fact that the blades are rotating, therefore, it is a function of the tip speed ratio $\lambda = \frac{\Omega R}{v_1}$, where Ω is the rotor speed in rad/s. Assuming a generic 3.5 MW wind turbine, with a rotor speed of 15 rpm ($\frac{\pi}{2}$ rad/s), rotor radius of 60 m, and a wind speed $v_1 = 15$ m/s, results in $\lambda = 2\pi$. Thus, from Figure 1.2 the thrust coefficient is $c_T = 0.8$, and from equation (1.1), taking $\rho_a = 1.2$ kg/m^3 (neglecting variation effects of altitude, air temperature, atmospheric pressure and relative humidity) the resulting thrust force on the hub is $F_T = 1.2$ MN. Note that for storm wind, say v_1

= 30 m/s, $c_T(\lambda = \pi)$ reduces to 0.3, resulting in an increase of F_T to 1.8 MN.

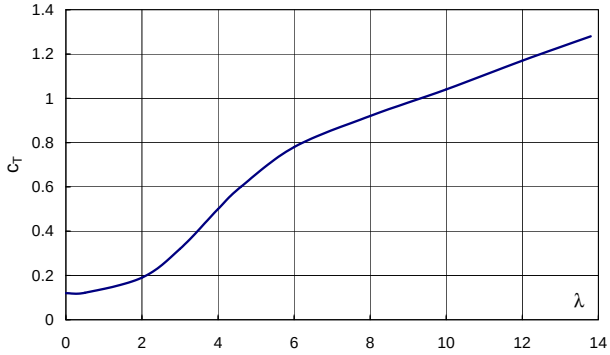

Figure 1.2: Thrust coefficient of a turbine as a function of the speed tip ratio (from Kühn, 2002)

Exact values will depend on the turbine design, nevertheless the above calculations are useful since they give the order of magnitude of the horizontal load applied at the hub level by the wind. More importantly note that the thrust force acts at a level that creates a very high moment at the foundation level (see Figure 1.6(a)).

1.1.4 Environmental load of the waves and currents

Waves induce vortices of water particles, which generate drag forces on obstacles. In addition, a fluid moving horizontally also generates pressures over obstacles. If a dominant extreme wave is idealized then hydrodynamic loads can be obtained from the drag and inertia forces applied on a submerged turbine tower as follows (Kühn, 2002):

$$F_D = \frac{C_D \rho_w (2R) H_s^2 \omega^2}{16\psi} \frac{\sinh(2\psi d_w) + 2\psi d_w}{\cosh(2\psi d_w) - 1} \tag{1.2}$$

$$F_M = \frac{\pi C_M \rho_w (2R)^2 H_s \omega^2}{8\psi} \tag{1.3}$$

where $C_D \approx 0.7$ and $C_M \approx 2$ are empirical coefficients for drag and inertia for smooth tubular sections, ρ_w is the water density, $2R$ is the tower diameter, H_s is the significant wave height, d_w is the water depth, $\omega = \frac{2\pi}{T}$ is the angular wave frequency and T is the wave period, and $\psi = \frac{2\pi}{L}$ is the 'wave number' with L being the wave length. The wave number can be obtained from:

$$\omega^2 = g\psi \tanh(\psi d_w) \tag{1.4}$$

in a deep water case $\omega^2 = g\psi$, where g is the acceleration of gravity. The drag force varies with time through a $\cos^2$ function whilst the inertia force varies with time through a sin function. Therefore, the total horizontal load H can be expressed by:

$$H = max\left\{F_D \cos^2(-\omega t) + F_M \sin(-\omega t)\right\} \quad \text{for} \quad -\frac{T}{4} \leq t \leq 0 \tag{1.5}$$

Figure 1.3 shows the kinematics and loads associated with a wave of 6.4 m height and 9.4 s period applied on a tower 3 m diameter and 10 m water depth. The bottom plot in Figure 1.3 shows that the maximum horizontal load is 0.45 MN and because the load acts at 10 m height, it results in a moment of 4.5 MNm on the foundation. Considering the following case: $2R = 6$ m, $d_w = 15$ m and an extreme wave $H_s = 12$ m and $T = 12$ s, results in a maximum drag force of 0.7 MN and a maximum inertial force of 2 MN. But because both loads are not in phase the maximum horizontal load is 2 MN, generating a moment of 30 MNm at seabed level.

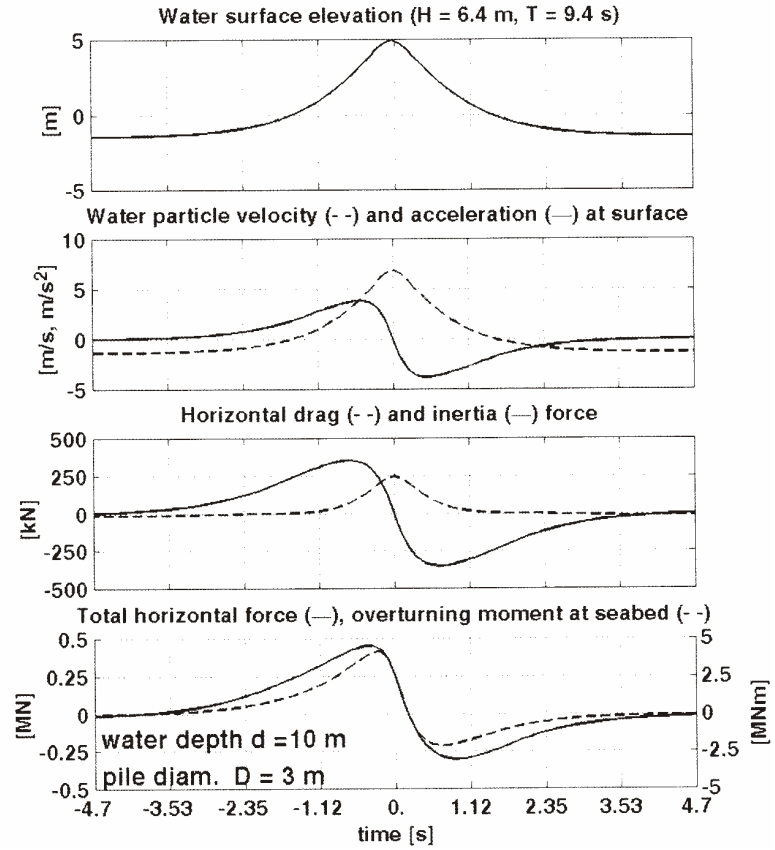

Figure 1.3: Kinematics and forces of an extreme wave in shallow water (from Kühn, 2002)

Shallow waters of 10 to 20 m can change dramatically with tidal range as in the Irish Sea

for example, where variations up to 8 m occur. Therefore, current induced forces should be included in the horizontal load. Apart from the horizontal load component, waves can induce an important vertical load component, pull and push during trough and crest respectively.

1.1.5 Seabed materials at the UK sites proposed

Table 1.3 gives a general description of the ground conditions in the UK sites proposed for the first round of wind farms. Figure 1.4(a) shows the seabed sediments in the Irish

Table 1.3: First round of wind farms in the United Kingdom

Area	Wind Farm	Site	Soil conditions sand over (clay over)	N°
Irish Sea	1 Robin Rigg	Solway Firth	medium & stiff clay	60
	2 Barrow†	Cumbria	medium & stiff clay	30
	3 North Hoyle†	North Wales	sand, bedrock & (bedrock)	30
	3 Rhyl Flats	North Wales	sand, medium & stiff clay	30
	4 Shell Flats	Lancashire	soft clay	90
	5 Burbo Bank	Liverpool Bay	sand, medium & stiff clay	30
Swansea Bay	Scaweather Sands	South Wales	(bedrock) & bedrock	30
Thames Estuary	Kentish Flats†	Kent	soft & stiff clay	30
	Gunfleet Sands	Essex	soft, medium & stiff clay	30
East Anglia / Skegness	Scroby Sands†	Norfolk	sand	30
	Cromer	Norfolk	medium clay & bedrock	30
	Inner Dowsing	Lincolnshire	medium clay & bedrock	30
	Lynn	Lincolnshire	medium clay & bedrock	30
Northeast	Teeside	Cleveland	bedrock & (bedrock)	30

†operating, N°: number of turbines

Sea and the sites of wind farms projected. There is mostly sand, corresponding to sand banks. These sand banks are underlain by clay, bedrock or simply sand continues deeper. However, there are also some sites with clay underlain by bedrock. A particular feature of the sand banks is their regular mobility caused by tides and currents. This phenomenon will cause sediment transport and scour, which will require a rip-rap or other form of protection around the suction caissons (HR Wallingford, 2004). This issue is not considered in this thesis.

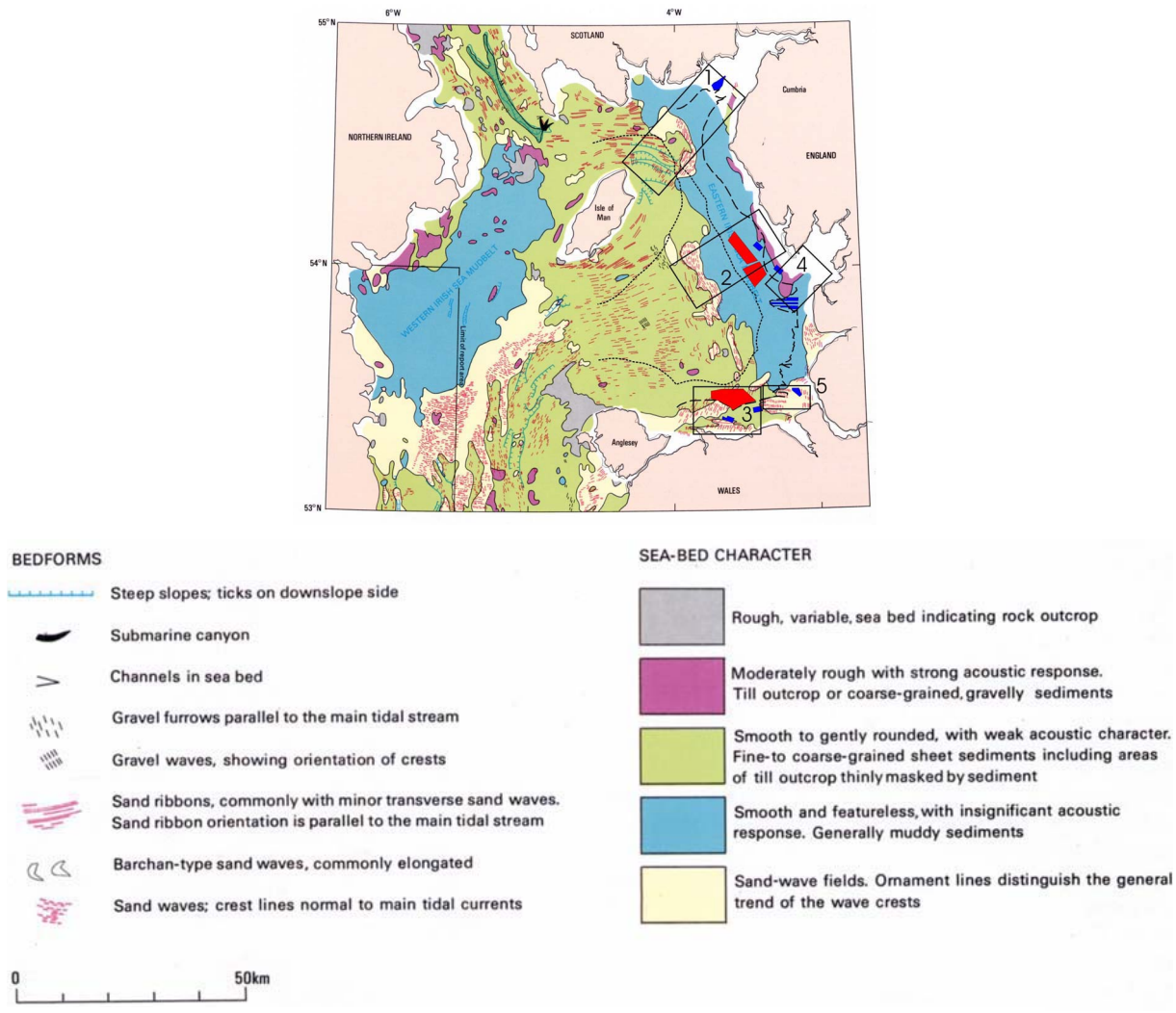

Figure 1.4: Seabed sediments in the Irish Sea, showing sites for offshore wind farm projects (British Geological Survey, 2004)

1.1.6 Existing foundation options for offshore wind turbines

According to Table 1.1 monopile foundations have dominated the offshore wind energy projects followed by gravity bases (see Figure 1.5(a)). It is important to realize that the increase of the turbine size above 3 MW implies larger loads acting on the turbine base, and hence, larger foundations. Indicative of this situation is the fact that the monopile diameters in the recent projects of Kentish Flats and Egmond are 4 m and 4.6 m respectively (Figure 1.5(b)), significantly larger than usual offshore driven piles. Moreover, the 5 MW world's largest wind turbine, the Beatrice offshore wind farm in the Moray Firth, Scotland, has been erected in 45 m water depth. The tower rests on jacket structures of 50 m height, which are founded on four piles (Figure 1.5(c)). Finally,

Figure 1.5(d) shows a very large reinforced concrete cylinder founded on piles for a 4.5 MW turbine project in Ems-Emden, Germany.

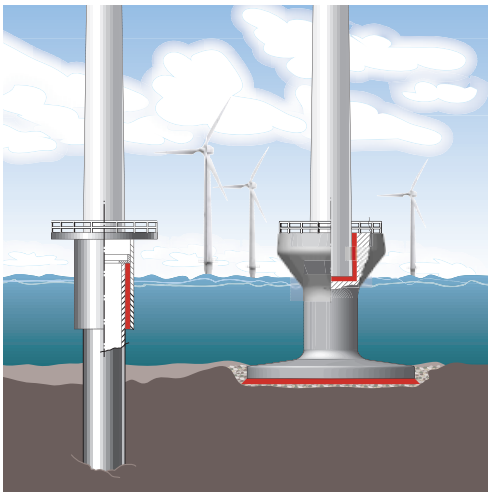

(a) Monopile and gravity base

(b) Monopile

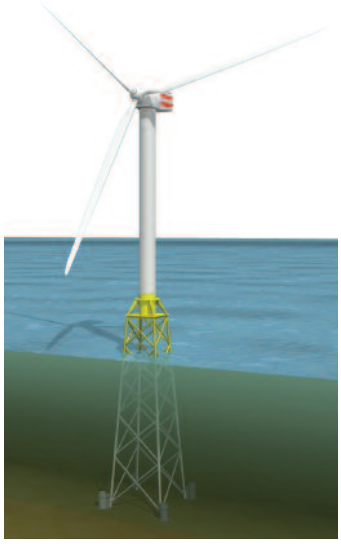

(c) Piled jacket tower

(d) Piled reinforced concrete cylinder

Figure 1.5: Existing foundation options for offshore wind turbines. Source: (a) www.densit.com, (b) www.kentishflats.co.uk, (c) www.beatrice.co.uk, and (d) www.enova.de

The existing foundation solutions adopted for large turbines seem to be cumbersome, time and resource consuming. As a result cheaper and simpler solutions are being sought by researchers and engineers. It has been proposed that suction caisson foundations, used previously as anchors in deep waters and as shallow foundations for oil rigs, might be a better alternative from the economic, technical and environmental point of view.

1.1.7 Suction caisson foundations

Suction caissons acquire the name from the fact that a *caisson* is a large water-tight box where the pressure inside differs from the atmospheric pressure. *Suction* corresponds to the negative pressure or underpressure applied inside the caisson to extract water and

in this way penetrate the caisson skirts into the ground. Because in shape they resemble an upside-down bucket, suction caissons have also been called suction buckets.

Suction caissons have demonstrated to be more efficient than piles, in terms of installation time in applications for the oil and gas industry (Andersen and Jostad, 1999). These issues acquire more importance in offshore applications where harsher weather conditions are prevalent. The efficiency in the installation of suction caissons relies on the use of pumps rather than large and heavy hammers used to drive piles, not to mention socketed and grouted piles, which require predrilled holes. Furthermore, suction caissons can be removed easily (by changing the suction to overpressure), making them more versatile and environmentally friendly, as compared with piled foundations.

Figures 1.6(a) and 1.6(b) show the two suction caisson configurations described by Houlsby and Byrne (2000) for offshore wind turbines. Figure 1.6(a) corresponds to a monopod suction caisson foundation, and Figure 1.6(b) depicts a multiple suction caisson foundation, tripod or tetrapod. Each configuration has a predominant loading system. In the first alternative the horizontal loads at the hub and at the wave-breaking level leads to a resultant overturning moment of 120 MNm which is transmitted directly to the foundation. Whilst in the second alternative the same moment is transferred through the lattice to the foundation as tensile and compressive vertical loads.

In the study of structure-foundation interaction problems attention should be paid to the substantial differences between for instance the jack-up problem and the wind turbine problem, as pointed out by Houlsby and Byrne (2000). Firstly, the water depth for oil and gas structures is much deeper than for wind turbines, in the order of 100 m for fixed structures and up to 2000 m for floating structures (Sparrevik, 2002). By contrast, the water depth at the sites designated by Crown Estates for the wind farm projects is between 10 m and 20 m. Secondly, the state of loading also differs since oil rigs are fairly heavy structures. Then gravity forces dominate over environmental forces. Conversely, offshore wind turbines are slender and light structures. Therefore, the environmental

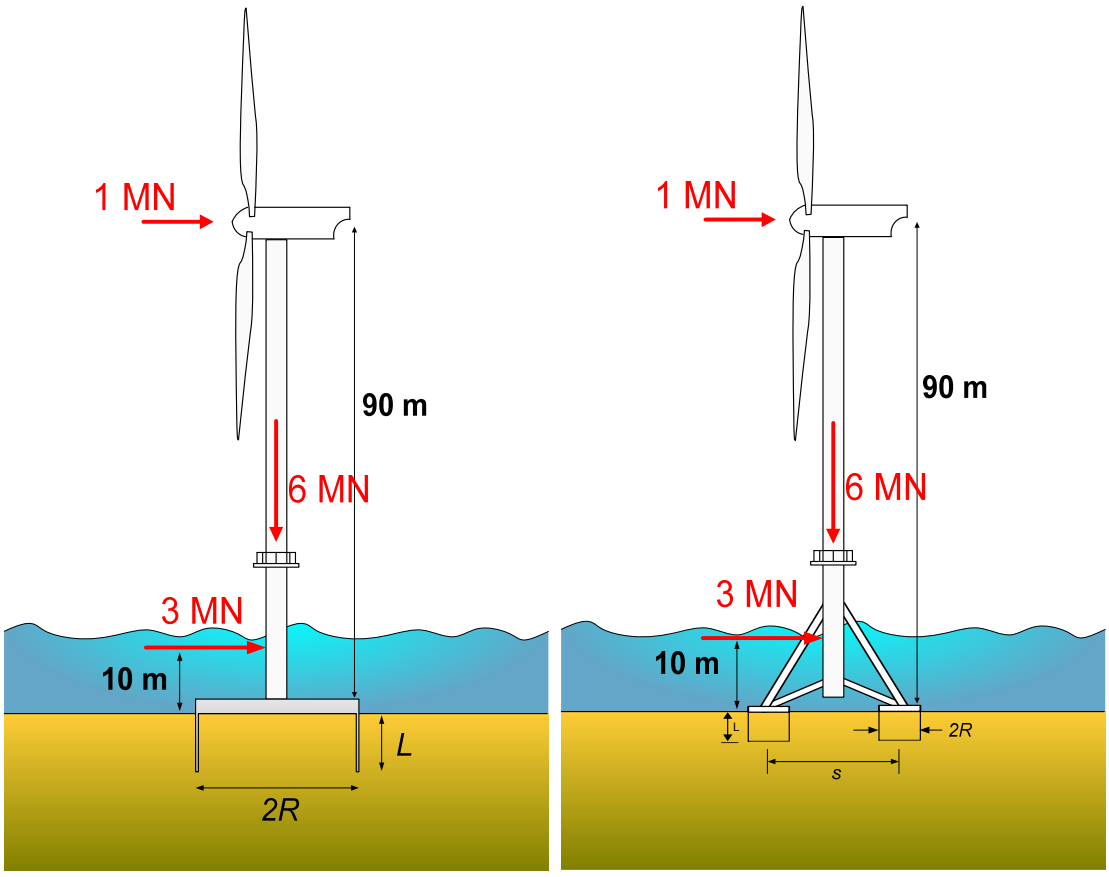

(a) Monopod suction caisson (b) Multiple suction caissons

Figure 1.6: Typical loads and dimensions for a 3.5 MW turbine showing different foundations

forces are much larger as a proportion of the gravity forces (Byrne and Houlsby, 2003). A comparison of typical extreme load values for a 3.5 MW wind turbine is shown in Figures 1.6(a) and 1.6(b).

It is important to highlight that the foundation cost has a strong influence on the total cost of offshore wind farm projects, typically being between 15% and 40% (Houlsby and Byrne, 2000). Feld *et al.* (1999) reported that the cost of the gravity base foundations at Vindeby and Tunø Knob represented 23% of the total costs of the wind farm. Feld *et al.* also determined that a tripod caisson reduces the footing steel by up to 34% in comparison with a tripod pile for the case of very hard clay (Rødsand), whereas for dense sand only 6% would be saved (Horns Rev). Moreover, Ibsen *et al.* (2003) indicated that in the Horns Rev project the foundation total costs comprised of 8% design, 46% steel and 46% installation. In addition, it was estimated that monopod suction caissons

can save up to 25% of steel compared with monopiles. However, an economic study carried out by Beresford (2003) contradicts the above estimate for the Kentish Flats and Solway Firth wind farm projects. Accounting only for the materials involved, Beresford (2003) determined that a monopile is the cheapest solution (*ca.* £80k) compared with: i) tetrapod piles (*ca.* £160k), ii) monopod caisson (*ca.* £400k in sand and *ca.* £300k in clay), and iii) tetrapod caissons (*ca.* £280k in sand and clay). However, the variable costs of installation can be easily equal or even higher than the fixed costs of materials and design. For instance, in the Scroby Sands project 30% of the foundation cost was equally split between fix and variable costs, without any unexpected delay owing to good weather. Variable costs were mostly controlled by the hire of a barge for £50k/day.

In October 2002 the first monopod suction caisson ($2R = 12$ m, $L = 6$ m) was installed into the sand of Frederikshavn. However, caisson foundations have not yet been installed offshore.

Finally, it is thought that a wind turbine could be completely assembled onshore and then transported and installed at once using suction caisson foundations. This possibility is an extraordinary advantage over the existing foundation options since it is an efficient use of time and resources.

1.2 SHALLOW FOUNDATION RESEARCH

1.2.1 Elastic behaviour

A compendium of linear-elastic solutions for flat, rigid footings resting on a homogeneous half space can be found in Poulos and Davis (1974), and a more instructive and pedagogic source in Davis and Selvadurai (1996). Bell (1991) and Ngo-Tran (1996) extended those solutions to the case of embedded footings. Using the scaled boundary finite element method Doherty and Deeks (2003) determine the solutions (stiffness coefficients) for *rigid caissons* embedded in non-homogeneous elastic soil. Subsequently, Doherty *et*

al. (2005) extend the analysis to caissons with *flexible skirts*. Elastic solutions are based on two soil parameters: the Poisson's ratio and the shear modulus. Whilst for the former values usually adopted are 0.5 for clays and 0.2 for sands, determination of the latter is not straightforward. From several resonant column tests conducted at small strain amplitudes reported by Hardin and Richart (1963) amongst others, it was found that the shear modulus varies with the specific volume and is a power function of the current level of stresses with exponent n. Mitchell and Soga (2005) present a summary of shear modulus functions for different type of soils with values of $n = 0.5 \pm 0.1$.

1.2.2 Bearing capacity and plasticity models

Methods of calculation based on Terzaghi (1943) bearing capacity formulation have been widely adopted in practice for the analysis of shallow foundations. This formulation superposes linearly the effects of soil cohesion, surcharge and weight. Meyerhof (1951), Brinch Hansen (1970) and Vesic (1975) developed methods that include factors to the original formulation to account for footing shape and depth; load inclination and eccentricity. Although these procedures of calculation are very similar, differences exist in the factor expressions. Furthermore, they are limited to the case of foundation collapse as a general shear failure, without providing information about previous or later stages of loading let alone footing displacements.

A different approach based on the concept of "yield" rather than "collapse" has been increasingly adopted by researchers. Houlsby and Byrne (2001) discuss the advantages of using a yield surface approach instead of the usual bearing capacity calculation approach. They point out that actually such an approach was initiated by Roscoe and Schofield in 1957 when envelopes of normalised forces were used to analyse the interaction between a steel frame and its foundations. So, the concept of force-resultant model was introduced by Roscoe and Schofield (1957), in which the structure response can be integrated with the foundation response and vice versa.

Embracing this concept Ticof (1977) carried out several series of load-controlled lateral loading tests on a flat, rough strip model footing resting on sand. He found that the data was well fitted by a symmetric parabolic envelope in the horizontal-vertical load $H - V$ plane, and an elliptical envelope in the moment-horizontal load $M - H$ plane. From these findings Butterfield and Ticof (1979) suggested a three dimensional "cigar shaped" yield surface in the $V - M - H$ space.

The cigar shaped yield surface was later verified by Georgiadis and Butterfield (1988) on dense, dry sand. Subsequently, Tan (1990) studied combined loading on saturated sand of conical and spudcan footings for applications to jack-up units in deep water. He established an analogy between the Cam Clay critical state model to analyse the response of soils in triaxial testing and the force-resultant model to analyse the combined loading of shallow foundations. Tan (1990) carried out "sideswipe" tests in the drum and beam centrifuges at Cambridge. A sideswipe test is defined as the application of horizontal displacement to a footing whilst keeping constant the vertical displacement, in analogy to an undrained triaxial test. Under certain conditions of foundation stiffness sideswipe events trace very closely the yield surface. Moreover, the concept of critical state in soils led to the concept of a parallel point or parallel line, which establishes the state of transition between settlement and uplift of a foundation. "Parallel" refers to the flow vectors being parallel to the H and M axis. Although, Tan proposed a non symmetrical yield surface and plastic potential, his study only included results in the $H - V$ plane, omitting moment and rotation from the analysis. Later Dean *et al.* (1992) continued Tan's (1990) work introducing moment into the analysis.

Nova and Montrasio (1991) performed load-controlled tests using a system of weights and pulleys to apply combined loadings to a *strip footing* on a loose, silica sand. From the test results a work-hardening plasticity model with a non-associated flow rule was constructed within what it was referred to as a macro-element framework . This plasticity model consisted of: i) an empirical hardening law obtained from vertical load-penetration tests, ii) a yield surface, and iii) a plastic potential. Elastic analysis was considered in-

adequate in predicting displacements during combined loading according to Nova and Montrasio (1991). Further tests using a *circular footing* on a dense sand were analysed by Montrasio and Nova (1997), concluding that the shape of the yield surface was not affected by the circular footing shape, but the shape parameters introduced vary linearly with the foundation embedment.

Further experimental support for a "cigar shaped" yield surface composed of parabolas and ellipses was provided by Gottardi and Butterfield (1993, 1995) and Butterfield and Gottardi (1994). A step forward was undertaken by Martin (1994), who designed and constructed an advanced three-degree-of-freedom (3DOF) apparatus able to apply to a footing simultaneously vertical, rotational and horizontal displacements $(w, 2R\theta, u)$ and obtain the corresponding loads (V, M, H). Martin conducted a comprehensive series of tests using spudcan footings on heavily overconsolidated Speswhite Kaolin clay. The testing programme included horizontal and rotational swipe events under various load ratios $\frac{M}{2RH}$ as well as moment and horizontal loading events under constant vertical load at different $\frac{M}{2RH}$ ratios. Martin concluded that the shape of the yield surface remained constant regardless of its expansion, the size of the yield surface increased with the footing penetration, and elastic behaviour occurred within the yield surface. Furthermore, a work-hardening plasticity formulation referred to as 'Model B' was developed, which was included in a structural analysis program suitable for the analysis of jack-up units. Overall, Martin's (1994) work encapsulates the complete construction and application of a force-resultant model based on experimental data. Details of model B appear also in Houlsby and Martin (1992) and Martin and Houlsby (1999, 2000, 2001).

The effect of loading rate was investigated by Mangal (1999), who conducted using Martin's 3DOF loading rig, *partially drained* loading tests using circular flat footings on a fine, oil-saturated sand. Mangal (1999) found in monotonic vertical loading tests (from velocities between 0.001 mm/s to 5 mm/s) that the initial foundation stiffness increased with rate. But after a penetration as small as $\frac{w}{2R} = 0.0003$ the stiffness reduced to values similar to those under drained conditions. From swipe tests with alternating slow and

rapid rates he found that the yield surface expands with rate. However, these experimental findings have not yet been interpreted within a rate dependent theoretical framework.

Using the 3DOF loading apparatus designed by Martin (1994), Gottardi *et al.* (1999) undertook a comprehensive programme of displacement-controlled tests using *circular flat footings* on dense sand with the purpose of developing work-hardening plasticity models. Based on the experimental results obtained by Gottardi *et al.* (1999) an extension of the modelling of spudcan footings for jack-ups on dense sands was carried out by Cassidy (1999) and Houlsby and Cassidy (2002). They developed a plastic potential function to define the flow rule. Association factors were introduced to account for strong non-associative response found in the experimental results. The constructed model, referred to as 'Model C', predicts the response of drained-monotonic combined loading. Based on experimental results reported Byrne and Houlsby (2001) using a flat footing on a crushable and very compressible carbonate sand, an extension of Model C was carried out by Cassidy *et al.* (2002). The implementation of a hardening law that is a function not only of the plastic vertical displacement, but also of the plastic horizontal and rotational displacements was found to improve the modelling.

Force-resultant models reduce the soil-footing interaction problem to the analysis of loads and displacements at one load reference point (LRP). Houlsby (2003) points out that changes of the LRP modify the moment, horizontal and vertical displacements, which in turn affect the value of the elastic stiffness coefficients and the parameter values of the yield surface. The reduction of the analysis to the LRP, ignoring the modelling of the soil, is a very useful simplification that allows the simulation of complex soil-footing interaction problems. Model B and Model C can successfully predict monotonic plastic behaviour. Force-resultant models have also been formulated for other geotechnical applications such as rock impacts and soil-pipe interaction (Nova and di Prisco, 2003). However, elasticity, loading rate effects and cyclic loading are not yet well modelled; the presence of localized stress effects, for instance the phenomena of liquefaction and scour can limit the applications of these models (Houlsby, 2003).

The extension of the yield surface formulation from planar loads to general loads, *i.e.* vertical load, two perpendicular moments, two perpendicular horizontal loads and torsional load, was proposed by Martin (1994). Houlsby (2003) extended model C to carry out a six-degree-of-freedom (6DOF) modelling of jack up foundations. Because of the necessity to verify experimentally 6DOF models, Byrne and Houlsby (2005) designed and constructed a spatial loading apparatus. Using the 6DOF apparatus, Bienen *et al.* (2006) report the results of spatial combined loading tests of a circular, rough flat footing on dry, loose sand. By means of horizontal, rotational and torsional swipe tests and radial displacement tests Bienen *et al.* assess the yield surface, the plastic potential and the hardening law. The parameter values of the yield surface agreed with the values obtained in previous 3DOF studies. The new yield surface parameter related with torsion was determined as well as the torsional association factor for the plastic potential. It was found that a higher degree of non-association was required to describe torsion. The proposed hardening law considered the contribution of the six plastic displacement components.

1.2.3 Research on suction caisson foundations

The search for improving anchorage systems for military submarine applications led to the idea that an inverted 'cup' subjected to vacuum might be a feasible solution (if not the only one) to the anchoring problem as considered by Goodman *et al.* in 1961. Suction installed skirted footings were not commercially used until 1980 (Senpere and Auvergne, 1982). However, it was in early nineties that extended use in mooring applications for floating production units took place. The first permanent suction caissons were installed in 1995, and nowadays there are more than 485 suction caissons installed worldwide (Andersen *et al.*, 2005). Although, Ibsen *et al.* (2003) report the suction assisted installation of a 12 m diameter caisson for a wind turbine in Frederikshavn, there is not yet an offshore installation for such an application. A summary of past laboratory research into suction caissons carried out around the world is presented in Table 1.4.

Senpere and Auvergne (1982) reported practical information related to suction pile installations in the North Sea. The soil conditions were a layer of five to six metres of dense sand overlying one or two metres of soft clay followed by stiff clay with caisson diameter $2R$ of 3.5 m, skirt length L of 9 m and skirt thickness t of 25 mm. For the Gullfaks C project Tjelta *et al.* (1986) presented field tests of a concrete suction caisson ($2R = 6.5$ m, $L = 22$ m and $t = 0.4$ m) installed into soft clay overlaying medium dense sand layers and clayey sands at a very high suction level with a maximum of 500 kPa. However, the caisson penetration of the Gullfaks C platform was mostly due to self-weight with little suction. The Draupner E (formerly Europipe 16/11) and Sleipner T jacket projects demonstrated the feasibility of suction caissons penetrating very dense sands, which was initially verified in field tests ($2R = 1.5$ m, $L = 1.7$ m, $t = 12$ mm) and in laboratory tests ($2R = 550$ mm, $L = 300$ mm). These examples of successful installation of suction caissons demonstrated not only that the caisson skirt penetration into very dense sand is achievable, but also that suction caissons are an economically advantageous alternative to piled foundations (Tjelta, 1994, 1995).

Dyvik *et al.* (1993) reported the performance a series of static and cyclic loading tests on soft clay using large caissons intended to work as a cellular foundation for a tension leg platform TLP and floating structures. Andersen *et al.* (1993) showed that predictions (obtained from limit equilibrium and FE analysis) of pullout agreed very well with the experimental results, and upper limit predictions of cyclic vertical displacements were closer to the experimental results than lower limit predictions. As a result, suction caisson foundations have been preferred over piles and drag anchors for fixed and floating offshore platforms and in a wide range of other oil and gas facilities (Andersen and Jostad, 1999).

Aldwinckle (1994) carried out a study of the suction installation problem in sand, where the pore pressure variation was estimated during the penetration of the skirt. A *pressure factor* was introduced to account for the variation of pore pressure inside and outside the caisson, variation created by the hydraulic gradient caused by the suction. It was determined that the pressure factor diminishes exponentially with the skirt penetration

Table 1.4: Laboratory research on suction caissons (adapted from Byrne, 2000)

Reference	Soil[1]	Footing geometry $2R$ (L), mm	Loading[2]	Test type[3]
Goodman *et al.*, 1961	M, C, S	79 (99), 89 (188)	m V	installation
Brown & Nacci, 1971	S	254 (44.5)	m V	pullout
Helfrich *et al.*, 1976	S	415 (250)	m V	pullout
Wang *et al.*, 1977	S, M, C	111 (9.5, 55) 140 (13, 70) 200 (14.5, 82.6) 337 (35, 162)	m V	pullout
Larsen, 1989	S, C	104, 204, 305 (450)	m,c H	pullout
Steensen-Bach, 1992	S, C	48 (80, 96, 160) 65 (108, 130, 216) 80 (133, 160, 266)	m V	pullout
Clukey & Morrison, 1995	C	152.5 (305)	m,c V, V:H	100g pullout
Rao *et al.*, 1997	C	75 (75, 112.5, 150)	m V	pullout
Whittle *et al.*, 1998	C	50.8 (51)	m V	pullout
Randolph *et al.*, 1998	MCa	45 (106)	m,c H, V:H	120g
El-Gharbawy, 1998	C	125 (250) 100 (400, 600) 50 (600)	m,c V, V:H	pullout
Watson, 1999	C, MCa SCa	60 (25)	m,c V, H, m,c V:H	100g 150g
Allersma *et al.*, 1999	S, C	60 (67)	m H	150g
Allersma *et al.*, 1999b	S, C	60 (70)	m, c V	150g
Byrne, 2000	S	100 (16, 33, 66) 150 (50) 300 (100)	m, c V:M:H m, c V	dry sand oil saturated
Feld, 2001	S	200 (50, 100, 150, 200)	m V:M:H	pullout
House, 2002	C,MCa C	30, 40 (120), 46 (100) 10.4, 15.9, 37.2 (302.6) 40 (15), 32 (27), 25 (45) 22 (61), 19 (71)	m, c V m,c V:H	120g installation pullout
Byrne & Cassidy, 2002; Cassidy *et al.*, 2004	C	60 (15, 30, 60)	m, c V:M:H	100g
Rauch *et al.*, 2003	C	102 (910)	m V	installation
Chen & Randolph, 2004	C	30 (120)	m V	100g
Tran *et al.*, 2004, 2005	S	100 (100), 70, 80 (140) 60 (60), 70 (120)	m V	installation 100g
Kelly *et al.*, 2003, 2004, 2006a, 2006b	S, C	280 (180), 150, 200 (100) 150, 200 (100)	m, c V c V:M:H	pullout

[1] **S**and, **C**lay, **M** as silt, and **Ca**lcareous; [2] **m**onotonic, **c**yclic, **V**ertical, **M**oment, and **H**orizontal; [3] experimental work at 1g, otherwise indicated

and increases with the permeability ratio, which is defined as the permeability of the soil inside the caisson divided by the permeability of the soil outside the caisson. The suction estimated by Aldwinckle (1994) agreed with experimental results obtained by Charles (1994). This work was continued by Houlsby and Byrne (2005b), who used theories for the analysis of open-ended piles, lateral earth pressure and bearing capacity to develop calculation procedures to design the installation of suction caissons.

The use of suction caissons for offshore wind turbines was mentioned as an alternative to gravity bases and piles by Ferguson (1998) and proposed by Houlsby and Byrne (2000) and Byrne (2000). One of the first studies of caissons for offshore wind turbines in sand was carried out by Feld (2001), who analysed the change in effective stresses (inside, outside and at the tip of the caisson skirt) due to the suction using a CPT approach. However, the tip resistance and the friction forces could not be related directly to CPT measurements of sleeve friction f_s and cone resistance q_c.

Byrne (2000) planned a testing programme in which the experimental results were interpreted within work-hardening plasticity models. To this end Byrne modified Martin's 3DOF apparatus to accommodate higher loads and wrote a computer program that enabled independent feedback control on each loading axis, using an updated data acquisition system. Results from horizontal swipe tests in dry sand under the same load ratio $\frac{M}{2RH}$ revealed that the induced rotation increases with the caisson aspect ratio $\frac{L}{2R}$, from zero for flat footings to a value close to the applied horizontal displacement $\frac{u}{2R}$ for $\frac{L}{2R} = 0.66$. Loads were normalised by V_u, the ultimate bearing capacity of a flat footing. The normalised lateral capacity was similar for flat footings and skirted footings regardless the aspect ratio ($0.16 \leq \frac{L}{2R} \leq 0.66$) for a normalised vertical load $\frac{V'}{V_u} \leq 0.08$. However, for $0.1 < \frac{V'}{V_u} \leq 0.21$ skirted footings had higher lateral capacity than flat footings. In moment swipe tests the applied rotation caused an increase of the horizontal displacements with $\frac{L}{2R}$. Nevertheless the moment capacity was practically independent of $\frac{L}{2R}$. Parameter values of the yield surface were determined for caissons, extending Gottardi *et al.*'s (1999) data for flat footings.

Byrne (2000) observed a striking result in cyclic vertical loading in very dense, oil-saturated sand, which was also found by Johnson (1999) for caissons and Mangal (1999) for flat footings, that little foundation stiffness degradation occurred. Furthermore, the loading rate had also little effect on the caisson response under high mean vertical loads ($V_m > 100$ N, $\frac{V'}{\gamma'(2R)^3} > 3$). As a consequence, it would be possible to deduce the transient

response studying only monotonic loading. Similar conclusions were drawn from cyclic moment loading tests under constant vertical load. In addition, the moment capacity was found to be a function of the constant vertical load. Moreover, hysteresis loops complied with Masing behaviour and Pyke's rules since backbone curves captured the cyclic response. From rapid pullout tests, it was observed that the tensile response became softer than in compression and the absolute maximum tensile capacity was reached at the cavitation limit of the pore fluid.

Kelly *et al.* (2003, 2004, 2006b) performed a testing programme to study the vertical response of multiple caisson foundations. The experiments made use of a model suction caisson in a pressure chamber. Two dense water-saturated sands were employed in addition to the operation of a computer-controlled hydraulic actuator which applies loads as high as 100 kN and allows vertical displacements as fast as 100 mm/s. Using a fine sand ($D_{10} = 0.075$ mm) multiple-amplitude cyclic loading tests at 1 Hz and a mean vertical load $V_m = 35$ kN (568 kPa), were performed with and without a pressure in the chamber of 200 kPa, which simulates 20 m of water depth. Results from these tests indicated that the pressure increases the excess pore pressure by exactly 200 kPa. As a consequence, the increase in water depth makes a caisson foundation under rapid pullout less vulnerable to cavitation. Moreover, the generated excess pore pressures $\Delta u'$ increased linearly with the applied vertical stresses $\Delta\sigma'_v$ at a ratio as small as $\frac{\Delta u'}{\Delta\sigma'_v} = 0.044$. No evidence of unloading stiffness degradation was observed in a test of 1000 cycles conducted at 35 kN $\pm$15 kN. The *incremental displacement* per cycle decreased with the number of cycles becoming very small after 200 cycles, and half of the *cumulative displacement* occurred also in the first 200 cycles. Pullout tests conducted at 5 mm/s and 100 mm/s revealed that the tensile capacity increases substantially with the extraction rate as well as with the pressure. However, the extraction distance required to reach those highest tensile loads increases as well. These results were used to validate the calculation procedure proposed by Houlsby *et al.* (2005c) to predict tensile loads under different rates. However, cyclic load histories experienced by the caisson before pullout can reduce significantly the tensile response. Such cases are not covered by the theory of Houlsby *et al.* (2005c).

Using a much finer sand (D_{10} = 0.007 mm) Kelly *et al.* (2004, 2006b) found that as the frequency increases (0.1 Hz, 1 Hz and 10 Hz) the caisson net penetration decreases for relatively similar packages of 'positive' cyclic loads. Additionally, $\frac{\Delta u'}{\Delta \sigma'_v}$ increased with frequency but to much higher values, namely 0.14 for 0.1 Hz, 0.25 for 1 Hz and exponentially for 10 Hz. The increase in excess pore water pressure was not only caused by the higher loading rates, but also by the much lower sand permeability, at least three orders of magnitude lower. For the experimental conditions chosen (positive loads and dense sands) it was concluded that for serviceability loadings the design is controlled by the foundation stiffness rather than by the ultimate resistance.

Recently, there has been growing interest in studying the installation of caissons into sandy soils. Sanham (2003) finds that the penetration rate depends on the suction level and the caisson weight. Using caissons of aspect ratios 1 and 1.3 and loose sand he finds that for the same caisson weight the higher the suction the faster the penetration (from 0.03 mm/s to 0.66 mm/s). Conversely, the caisson weight did not influence the penetration rate. Tran *et al.* (2004) installed caissons at very high penetration rates, namely 0.3 mm/s and 6.5 mm/s. Surprisingly, piping failure did not occur. Despite the large amounts of flow generated by the extremely rapid penetrations, it was found that the soil plug heave was less than in slow penetration tests. It was suggested that most of the large upward flow generated occurred next to the skirt wall, disturbing substantially only the soil near the skirt. Results from mini-cone penetration tests carried out by Tran *et al.* (2005) before and after the suction installation gave evidence of relative density reductions from 91% to 50% (though around the centre and not next to the skirt), which in turn reduced the permeability to half.

Field trials have been less reported since they are more expensive than laboratory testing. Also, field trials are more complicated since there is less variation and accurate control over the soil and loading conditions. However, information from field trials represents an invaluable opportunity to compare laboratory results and calibrate models. For oil and

gas structure applications, ten field trials of suction caisson have been reported according to Byrne (2000). For wind turbine applications, Ibsen *et al.* (2003) described the installation and lateral loading trials of large scale suction caissons ($2R = 4$ m and 2 m, $\frac{L}{2R} = 1$) in Frederikshavn, site of the first installed prototype monopod caisson (section §1.1.7). Ibsen *et al.* mentioned that when critical suction was reached, piping in the sand adjacent to the skirt occurred, which halted irreversibly further penetration of the caisson.

Houlsby *et al.* (2005a, 2006) have reported two field trial programmes: at Bothkennar for clay and at Luce Bay for sand. The field trials were designed to install by suction large suction caissons and to subsequently apply monotonic and cyclic load paths. A hysteretic response was found from cyclic moment tests, evidence was found of gapping under large rotations and decay of the secant stiffness with the increase of rotation amplitude occurred. The tensile capacity obtained from pullout tests was limited by the capacity of the equipment. Kelly *et al.* (2006a) carried out tests to shadow the above field test results to study scale effects. Normalisation procedures were proposed for caisson stiffness and capacity. The derived scaling relationships performed better for small displacements rather than for large displacements.

Ibsen *et al.* (2005) reported the monitoring of deformations and pore pressures in the monopod caisson foundation in Frederikshavn. Measurements on the Vestas V90 3 MW turbine considered natural frequencies in operational mode, idling conditions, turbine without blades and nacelle. During operation the first mode of vibration was around 0.3 Hz (rotor excitation between 10 and 20 rpm) and the second mode between 0.5 and 1 Hz corresponded to the rotation of the blades. Knowledge of the excitation frequencies of the structure is fundamental, since the foundation design should avoid undesirable deformations due to resonance.

1.2.4 A new theoretical approach

Theoretical research based on finite element analysis and upper and lower bound theorems has been mostly dedicated to caissons in clayey soils. Those analysis as well as work-hardening plasticity models such as Model B and Model C have been limited to the modelling of monotonic behaviour. Although multiple yield surface models implemented within plasticity theory can cope with cyclic behaviour, these models become inevitably more complex with several parameters to determine. A new theory based on the work of Ziegler (1977, 1983) makes it possible to derive complete constitutive models from only two potential functions. Houlsby (1981) used this theory to derive plasticity models such as the modified Cam Clay model. The derived constitutive models automatically respect the first and second law of thermodynamics. This theory has been entitled *hyperplasticity* and has been further extended by Collins and Houlsby (1997) and Houlsby and Puzrin (2000). Hyperplasticity theory has been recently adopted by Nguyen-Sy (2006) to derive a model to analyse circular shallow foundations in three dimensions. Nguyen-Sy (2006) first validated the hyperplasticity model called ISIS, analysing monotonic loading of flat and spudcan footings on clay and sand to subsequently compare these results with results from Model B and Model C. This version of ISIS considered one yield surface, three dimensions and rate independence. To study cyclic behaviour a discretization of the continuous hyperplasticity model was performed, introducing a finite number (rather than infinite) of yield surfaces and mixed isotropic-kinematic hardening functions following Puzrin and Houlsby (2001, 2003). Isotropic hardening expands or contracts the current yield surface, whereas kinematic hardening translates the yield surface. An expression of the yield surface that can incorporate tensile capacity, which indeed suction caissons possess, was proposed by Nguyen-Sy and Houlsby (2005). The multiple-yield-surface model ISIS proved to be powerful in modelling Masing hysteretic behaviour of cyclically rotated caisson foundations.

1.3 THE NEED FOR MORE RESEARCH

Significant research has been recently devoted to the study of multiple caisson foundations (tripods and tetrapods), thanks to the work of Kelly *et al.* (2003, 2004, 2006b). Rather less attention has been paid to monopod caisson foundations. Investigation of tetrapod foundations has mainly concentrated on dense sands and positive cyclic vertical loadings. Additionally, the effect of suction installation has not yet been included. Moreover, transient loading of caissons in clay at low mean vertical loads, which includes negative cyclic loading, has not yet been covered by field or laboratory testing programmes. Furthermore, according to Table 1.4 the majority of the past laboratory work has covered ratios $\frac{V'}{\gamma'(2R)^3}$ greater than 1, whereas in the offshore wind problem that ratio is less than 1. Previous research considered principally high levels of V' compared with H and M, since applications were intended to be for heavy oil rigs.

Although preliminary studies provide valuable information, for instance Tran *et al.* (2004) describe effects of penetration rate caused by different suction levels applied, it is necessary to interpret experimental results within a theory able to capture the variables that influence the load-penetration response.

The studies of suction caissons have been limited to consider a sequence of different load paths. Some studies have disregarded completely the installation process. Moreover, the complete vertical loading response, including failure and post failure, has not yet been studied. Assessment of the effects of installation method, by pushing and by suction, on subsequent vertical and moment loading has not yet been considered. Although the tensile capacity has been extensively studied in sand, it has been neglected in the analysis of the yield surface; instead the yield surface for flat footings or spudcan footings has been adopted. Furthermore, since swipe tests involve only deviatoric displacements (rotational and horizontal) the studies of the flow rule have overlooked the vertical displacement variation.

No explanation has been given for the absence of loading rate effect in cyclic vertical loading tests. Interpretation of the excess pore pressures developed during the cycles is required, since it has been shown by Byrne (2000) that in dense sands pore pressure build up can cause a softer response without losing considerable strength, whereas in loose sands stiffness degradation is highly likely to occur. However, it is not known whether the developing of suction inside the caisson may impede any degradation or not.

Finally, Nguyen-Sy (2006) demonstrated that hyperplasticity is a powerful theory in the modelling of cyclic behaviour of shallow foundations. This thesis attempts to provide physical understanding by means of experimental results. The results will be interpreted using a theoretical model. This will allow the determination of parameter values within hyperplasticity models, and their subsequent validations. Comparisons with results obtained from tests with large scale caissons will be also pursued, in particular from the programme of testing performed by Houlsby *et al.* (2005a, 2006).

1.3.1 Research objectives

The objective of this thesis was to contribute to the construction of hyperplasticity models for the analysis of suction caisson foundations. This objective is aimed to the

(a) 2R = 0.2 m, W = 30 N (b) 2R = 3 m, W = 20 kN (c) 2R = 12 m, W = 1.4 MN

Figure 1.7: Caisson footings showing diameter 2R and weight W: (a) in the soil mechanics laboratory, (b) in the field site at Bothkennar, and (c) at Frederikshavn, taken from www.hornsrev.dk

development of design procedures for caisson foundations for offshore wind turbines. To accomplish this objective, it is necessary to extrapolate laboratory results not only to field trials, but obviously to prototype foundations. Figures 1.7(a), 1.7(b) and 1.7(c) illustrate three size and weight of caissons. The first corresponds to a model caisson tested in the laboratory that can be held with the hands. The second is a model caisson tested in the field that is easily moved with one crane. The third is a caisson foundation for an offshore wind turbine moved with three cranes.

In order to extrapolate the results from the laboratory to prototypes loads, displacements, pore pressure, stiffness, *etc.* will be normalised along this thesis using scaling expressions derived from dimensional analysis.

Chapter 2

SOIL SPECIMENS AND APPARATUS

Abstract

This chapter describes the main properties and characteristics of the soils used in the experiments. The preparation of soil specimens are also described. Descriptions of the model caissons designed are presented, and boundary conditions are explained. Finally, the loading apparatus is described.

2.1 SOIL SPECIMENS MODELLED

Two types of *dry* sand have been used in this investigation to study drained behaviour: Dogs Bay and White Leighton Buzzard. For the study of partially drained and undrained behaviour two other sands have been used in *fully saturated* conditions: Baskarp Cyclone and Redhill 110. A further series of undrained tests were carried out in the extensively used and studied Speswhite kaolin clay. Standard laboratory tests were deemed unnecessary since properties of these soils have been characterised in a number of previous experimental studies undertaken at the University of Oxford and elsewhere. The soil properties are summarised in Tables 2.1 and 2.3 for the sands and the clay respectively. Figure 2.1 shows the grading curves for the sands.

Table 2.1: Properties of the different sands used in the experiments

Property	Dogs Bay (Nutt, 1993)	Leighton Buzzard (Schnaid, 1990)	Baskarp Cyclone (Mangal, 1999; Byrne, 2000)	Redhill 110 (Kelly *et al.*, 2004)
Mineralogy	carbonate	silica	silica	silica
D_{10}: mm	0.11	0.63	0.018	0.08
D_{30}: mm	0.18	0.70	0.038	0.10
D_{50}: mm	0.24	0.80	0.058	0.12
D_{60}: mm	0.29	0.85	0.069	0.13
C_u	2.66	1.36	3.87	1.63
C_c	1.00	0.92	1.16	0.96
G_s	2.75	2.65	2.69	2.65
$\gamma_{d\,min}$: kN/m^3	9.52	14.65	12.72	12.76
$\gamma_{d\,max}$: kN/m^3	13.60	17.58	16.85	16.80
υ_{min}	1.984	1.479	1.566	1.547
υ_{max}	2.834	1.774	2.075	2.037
ϕ'_{cs} : (°)	40.3	33	32.5	36

2.1.1 Dogs Bay sand

This is a biogenic carbonate sand from the west coast of Ireland and as can be observed in Figure 2.2(a), consists of a large proportion of broken skeletal mollusc fragments in the form of plates, hollow globules and tubes with the carbonate content ranging from 87% to 92% (Evans, 1987). It is a problematic soil in the sense that its angular particles can lead to high initial specific volumes. Moreover, it is a brittle material that breaks easily under load; since it is uniformly graded the breakage of particles is maximised (Coop *et al.*, 2004). However, Nutt (1993) found that the influence of the breakage on the internal friction angle is negligible. Therefore, in this series of tests the grading curve was not checked after testing to assess breakage. In Figure 2.1 only the initial grading is depicted. For more details about this carbonate sand see Nutt (1993).

2.1.2 White 14/25 Leighton Buzzard sand

This is a very uniform silica sand that has been widely used in research. The solid grains have sub-angular to sub-rounded shapes, composed of mostly quartz minerals (Figure 2.2(b)). The sand used corresponds to the 0.6 - 1.18 mm fraction, which is often referred to as 14/25 because it passes between the British Standard No 14 and No 25 sieves. Further details on the mechanical properties of this sand can be found in Schnaid

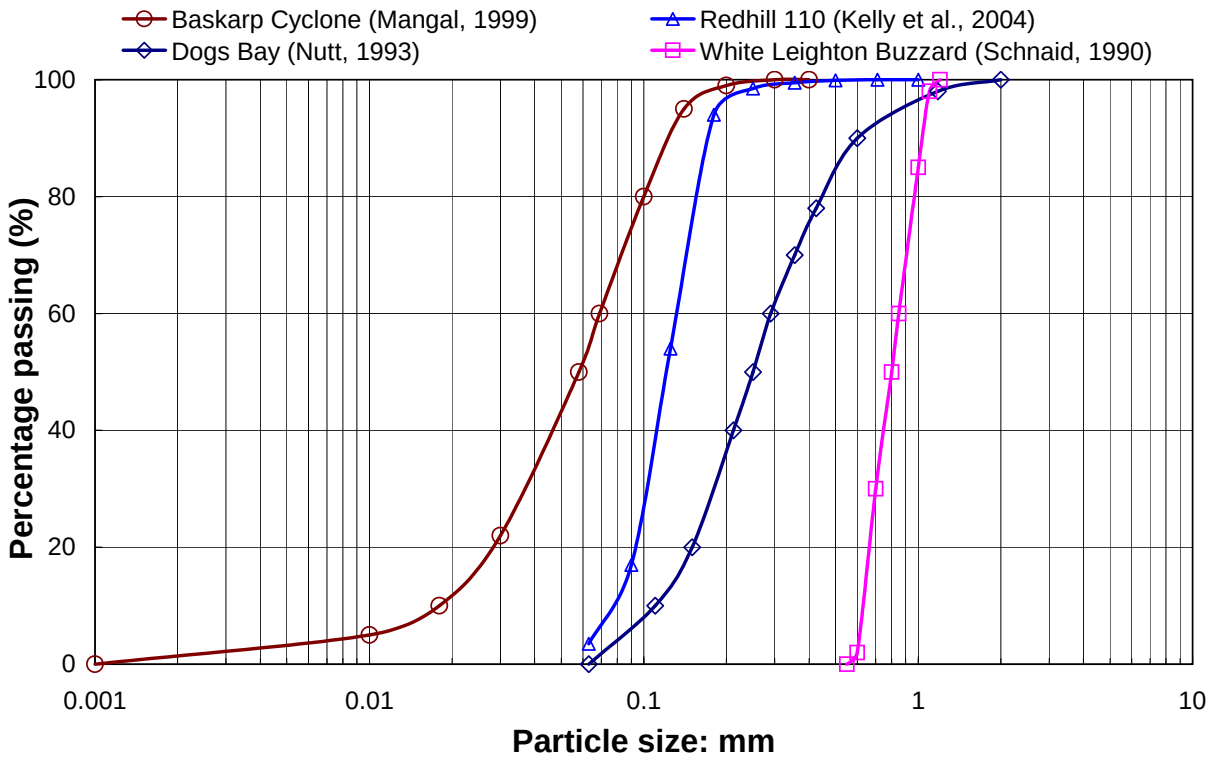

Figure 2.1: Particle size distribution curves for the cohesionless soils used in the experiments

(1990).

2.1.3 Baskarp Cyclone sand

This sand comes from a Holocene deposit in the southwest of the lake Vättern, north of Jönköping, Sweden. The sand is very fine as a result of a cyclone separation system (AB Baskarpsand of Habo). The sand consists of 84% quartz and the grains are angular to sub-angular as can be observed in Figure 2.2(c). The election of this fine sand is based on the fact that the simulation of partially drained and undrained behaviour is possible. When the sand is saturated by silicon oil the drainage times of offshore foundations can be modelled appropriately in the laboratory. The silicon oil used had a kinematic viscosity of 100 centistoke, *i.e.* 100 times more viscous than water. The coefficient of permeability is defined by:

$$k = K\frac{\gamma_f}{\mu_d} = K\frac{g}{\mu_k} \tag{2.1}$$

where K is the absolute permeability which indicates how *permeable* a porous material will be to *any* flowing fluid. The dynamic or absolute viscosity μ_d (Pa·s, Ns/m^2), is related

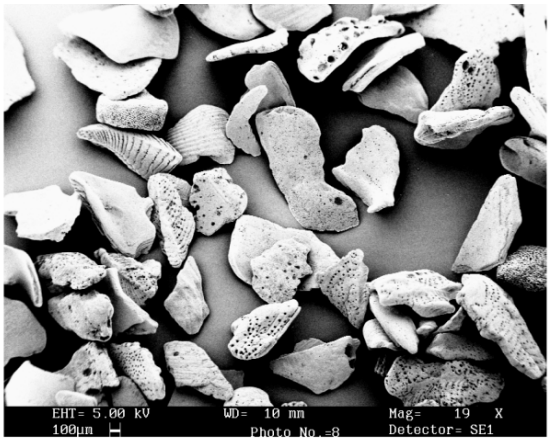

(a) Dogs Bay sand

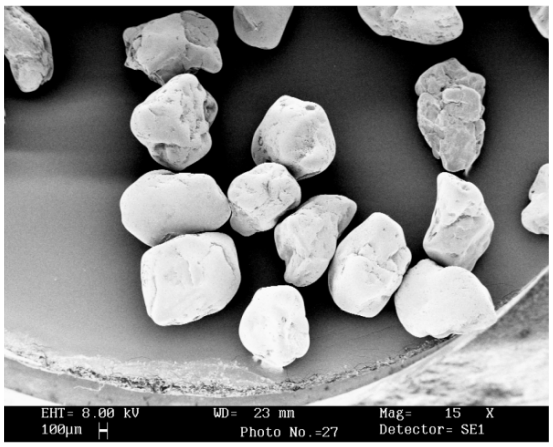

(b) Leighton Buzzard sand

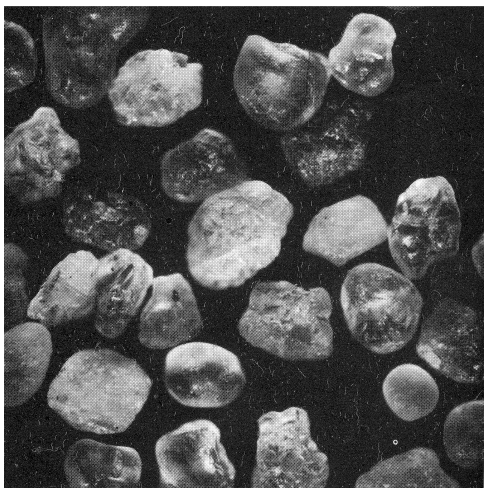

(c) Baskarp sand

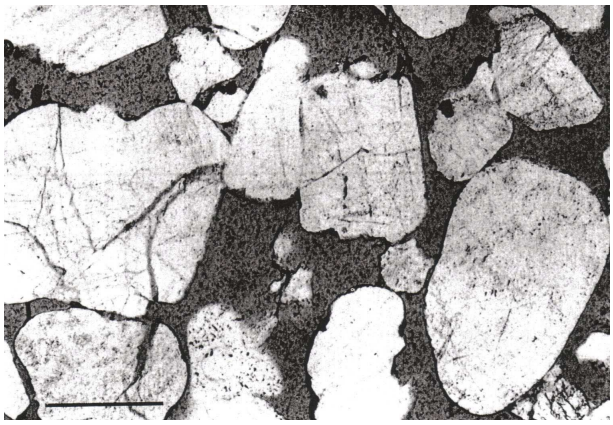

(d) Redhill sand

Figure 2.2: Photographs taken by: (a) Bowman *et al.* (2001) (b) Sentenac *et al.* (2001), (c) Per Karmhagen of Askania AB (no scale bar provided), and (d) Richards and Barton (1999), (the scale bar is approximately 0.3 mm in length)

with the kinematic viscosity μ_k (m^2/s), by means of $\mu_k = \frac{\mu_d}{\rho_f}$. Then, the coefficient of permeability for a sand saturated with silicon oil k_{oil}, can be found by taking the proportion of the coefficient of permeability for water k_{water}, using (2.1) for the same temperature (25°C for example), which results in:

$$k_{oil} = \frac{\mu_{k\,water}}{\mu_{k\,oil}} k_{water} \tag{2.2}$$

The coefficient of permeability of the Baskarp Cyclone sand with a relative density of 80% and saturated with water is $8{\cdot}10^{-6}$ m/s (Mangal, 1999). For the case of saturation with oil, the values of kinematic viscosity μ_k, given in Table 2.2, and according to equation (2.2), k_{oil} is expected to be around hundred times lower than k_{water}, to be precise $\frac{k_{water}}{k_{oil}}$

= 111. However, Mangal suggested a $k_{oil} = 1.8{\cdot}10^{-7}$ m/s for the oil-saturated Baskarp Cyclone sand with a relative density of 80%, which is only 44 times lower than k_{water}. This disparity might be attributed to temperatures different to 25°C during permeability measurements.

Table 2.2: Silicon oil and water properties (after Mangal, 1999 and Byrne, 2000)

Property	oil	water
Kinematic viscosity, μ_k at 25°C, cs: mm^2/s	100	0.897
Specific gravity, G_s at 25°C	0.96	1
Bulk modulus, B (for $\epsilon < 1\%$): MPa	800	2200

2.1.4 Redhill 110 sand

Geologically this sand belongs to the Folkestone beds, which are marine shallow-water deposits of Cretaceous age. It was obtained from Redhill, one of the exposures around the Lower Greensand outcrop in the southeast of England. Commercially produced (WBB Minerals), Redhill 110 is a high silica sand with a total quartz content of 98.8%. Redhill 110 is a fine sand with angular grains, as observed in Figure 2.2(d), and has similar coefficient of uniformity and curvature to those of the Leighton Buzzard sand. The coefficient of permeability for a water-saturated sample was estimated by Kelly *et al.* (2004) to be $k = 1.5 \cdot 10^{-4}$ m/s. On one hand the high imperviousness of the oil-saturated Baskarp Cyclone sand specimens is appropriate in modelling transient response, but on the other hand it takes long time to complete, for instance a caisson installation by suction. To avoid difficult interpretation of test under non-disipated pore pressures Baskarp Cyclone sand was replaced with the Redhill sand, which due to its larger coefficient of permeability allow drained conditions.

2.1.5 Speswhite kaolin clay

Speswhite kaolin clay has been used in numerous studies because its high permeability for a clay allows rapid consolidation of large specimens from reconstituted slurry. Characteristics taken from de Santa Maria (1988) and Martin (1994) are summarised in Table 2.3. It will be assumed here the shear strength distribution with depth proposed

Table 2.3: Representative Speswhite kaolin clay properties (after de Santa Maria, 1988 and Martin, 1994)

Property	Value
Specific gravity, G_s	2.61
Average effective unit weight, γ'	6.85 kN/m^3
Average moisture, w	50%
Liquid limit, LL	65%
Plastic limit, PL	34%
Coefficient of permeability, k ($p' = 200$ kPa)	$3{\cdot}10^{-9}$ m/s
Coefficient of consolidation, c_v ($p' = 200$ kPa)	0.3 mm^2/s

by Wroth (1984). The expression that Wroth (1984) postulates for this distribution is well supported by the results of undrained triaxial compression tests on isotropically consolidated specimens of reconstituted kaolin. Assuming that normally consolidated and overconsolidated specimens will reach the same *critical state point*, the shear strength can be written as:

$$s_u = \sigma'_v \left(\frac{s_u}{\sigma'_v}\right)_{nc} \mathrm{OCR}^{\Lambda} \tag{2.3}$$

where $\left(\frac{s_u}{\sigma'_v}\right)_{nc}$ is the shear strength ratio for normally consolidated clays, $\sigma'_v = \gamma' z$ is the vertical stress, $\mathrm{OCR} = \frac{\sigma'_{v_o}}{\sigma'_{v_i}}$ is the overconsolidation ratio with σ'_{v_o} the maximum vertical stress in the consolidation process and σ'_{v_i} the stress once the consolidation load has been removed. Λ is a parameter established in CSSM to indicate the relative slopes of the normal compression λ, and unloading-reloading κ lines for the soil.

$$\Lambda = \frac{\lambda - \kappa}{\lambda} \tag{2.4}$$

The consolidation procedure described below in §2.2.5 implies an OCR variation with depth of the form

$$\mathrm{OCR} = \frac{\sigma'_{v_o}}{\sigma'_{v_i}} = \frac{\Delta\sigma'_v + \gamma' z}{\gamma' z} \tag{2.5}$$

where $\Delta\sigma_v$ is the consolidation pressure. Thus, the shear strength gradient becomes

$$\frac{ds_u}{dz} = \gamma' \mathrm{OCR}^{\Lambda} \left(\frac{s_u}{\sigma'_v}\right)_{nc} \left[1 - \frac{\Lambda}{OCR} \frac{\Delta\sigma'_v}{\gamma' z}\right] \tag{2.6}$$

The submerged unit weight of the clay specimen can be estimated from

$$\gamma' = \left(\frac{G_s - 1}{wG_s + 1} \right) \gamma_w \tag{2.7}$$

where G_s is the specific gravity. The water content w, can be expressed in terms of the undrained shear strength s_u, as shown in Figure 2.3, in which the group of data where s_u $<$ 20 kPa corresponds to Martin (1994) and the data for s_u $>$ 20 kPa to Smith (1993). The data referred to as stressed corresponds to vane tests on clay subjected to vertical and radial stresses in a 1 m diameter calibration chamber. The following relationships have been obtained from best fits of the results from vane shear tests performed by both authors.

$$w = 67.192 - 6.535 ln s_u; \quad \upsilon = 2.754 - 0.171 ln s_u \tag{2.8}$$

From the second expression in (2.8) an analogy with compression and critical state lines

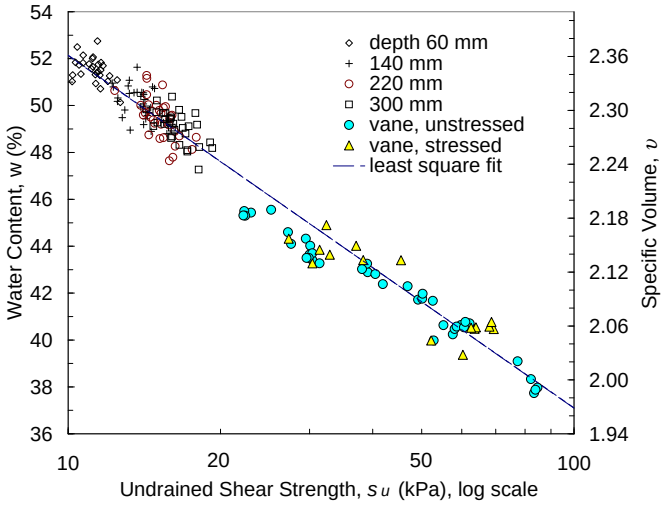

Figure 2.3: Undrained shear strengths and corresponding water content. Adapted from two series of shear vane tests: depth from 60 to 300 mm (Martin, 1994) and stressed and unstressed (Smith, 1993)

can be postulated in relation with the slope magnitude $\lambda = 0.171$ in the $\upsilon - lnp'$ plane. In this investigation, the shear strength was measured at 25 mm and 125 mm depth with a shear vane apparatus mentioned later on in §2.2.5. Table 2.4 presents these results in the form of averaged s_u. To appreciate the idealized distribution of s_u with depth, Figures 2.4(a) and 2.4(b) illustrate the averaged values together with error bars. The

Table 2.4: Shear strength from shear vane tests and parameters for profile estimation

Tank (sample)	$s_{u_{25}}$ kPa	$s_{u_{125}}$ kPa	$\left(\frac{s_u}{\sigma'_v}\right)_{nc}$	Λ
1‡ (1)	4.6	7.3	0.19	0.70
2 (2)	5.1	8.1	0.21	0.70
2_2 (2)	4.6	7.3	0.19	0.70
2‡ (5)	5.7†	6.1†	0.23	0.71
3 (3)	6.7	10.2	0.26	0.70
3‡ (6)	4.5	8.4	0.22	0.70
4 (4)	8.8	13.2	0.35	0.70
4‡ (7)	6.3†	9.9†	0.22	0.73

‡specimen inverted, †back calculated

fluctuation is rather small and is hardly visible in some of the points. An explanation of the inverted specimens will be also found in §2.2.5. Figures 2.4(a) and 2.4(b) depict the strength profile estimated using (2.3) together with (2.5), (2.7). The values of $\left(\frac{s_u}{\sigma'_v}\right)_{nc}$

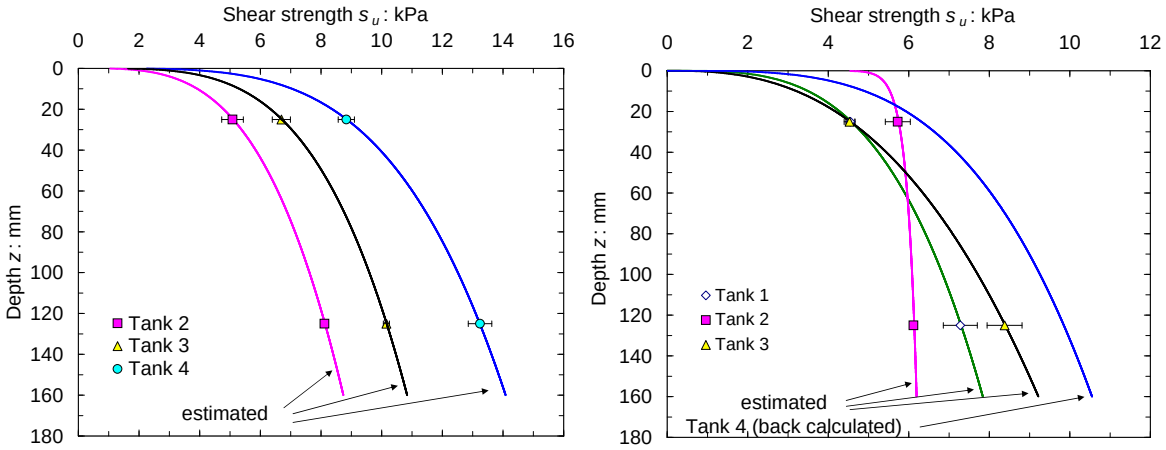

Figure 2.4: Vertical profiles of undrained shear strength (a) top of the sample (b) bottom of the sample (inverted)

and Λ were obtained from the best fit of (2.3) to the averaged experimental points of s_u. These profiles will be used in subsequent calculations, for instance, in the study of the vertical load required to install suction caissons.

2.2 SAMPLE PREPARATION

2.2.1 Dry Dogs Bay and Leighton Buzzard sands

The sand used during the testing was placed in a large aluminium tank with diameter 1100 mm and depth 250 mm. It had a rim at the top to which a loading apparatus and any other equipment could be attached as shown in Figure 2.10(a). A deeper sample of 400 mm was made possible by bolting on an additional 150 mm aluminium ring.

In the bearing capacity tests (Chapter 3), a total of five different relative densities were reached, four with the silica sand and one with the carbonate sand. Three loose samples of soil were prepared by carefully placing the sand into the tank from a scoop, keeping the drop height to a minimum. This method enables very loose sand samples to be prepared with relative densities of 26% for the Dogs Bay sand, and 40% and 47% for the Leighton Buzzard sand. For the denser samples only the Leighton Buzzard sand was used. A process of vibration was used until a high relative density ($R_d = 80\%$) was reached. This density was obtained after few minutes of vibration using a vibrating motor (Viking Vibramotor CUB 52B, 5000 N force, 3000 rpm, rated output of 180 W, and motor mass of 13 Kg) attached underneath the tank. To control the sample density measurements of the sample thickness were carried out in several places on top of the sample, knowing a priori the weight of the sample. To obtain an even denser sample a surcharge ($\approx$ 2 kPa) was placed on the sample in the form of lead weights (Lau, 1988). Attention was payed to not apply excesive vibration since this may induce non-uniformity of the sample, densifying more the top layer. Therefore, vibration was halted once no significant variation of the specimen thickness was meassured.

A series of moment loading tests was carried out only in loose Leighton Buzzard samples following the preparation procedure above described. The mean relative density of the samples was 22%, values determined in each test are summarised in Tables 4.1 and 4.2. Densities were measured before testing by weighing the sand within the tank and determining the volume of the sample. The relative density was calculated assuming the values

of minimum and maximum specific volumes shown in Table 2.1, which were obtained by the authors shown in same table.

2.2.2 Oil-saturated Baskarp Cyclone sand

A watertight tank with a filter at the bottom, a drainage system and filled with 250 mm height of Baskarp Cyclone sand under a column of oil between 60 mm and 120 mm was used for partially drained and undrained testing (see Figure 2.13). Sample preparation followed the procedure suggested by Mangal (1999) and Byrne (2000). According to these procedures, firstly, the sample of oil-saturated sand was stirred with a device (stirrer) - developed by the above authors. The stirrer was attached to the tank rim and a rotating paddle was lowered at a very slow rate (0.1 - 0.03 mm/min) from the surface to 150 - 200 mm in depth. The paddle suspended the particles of soil allowing fluidisation of the sample and forming a homogeneous sample simultaneously. Putting the fluid containment tank shown in Figure 2.13 around 0.3 m above the fluid surface in the tank with the sample created a head which in turn applied an upward flow. In this way effective stresses were reduced. After five days of stirring, densification occurred by sedimentation of the fluidised particles in addition to vibration of the sample. The vibration was carried out using a vibrator motor attached underneath the tank. The vibration was applied in a range of 2 to 3 hours, which is a much longer period than that applied to dry sand. The fluid containment tank was located around 0.3 m below the fluid surface to create a hydraulic gradient, which resulted in a downwards flow. The vibration and the downward hydraulic gradient arrange the sand grains into a denser packing. The cone resistance q_c was estimated by driving a small cone penetrometer into the sample at a tested site. Mangal (1999) proposed an empirical expression of the relative density R_d (in %) related to q_c as follows:

$$R_d = \frac{1}{0.11} ln \left(\frac{q_c}{0.044} \right) \qquad q_c \text{ in kPa and at 75 mm penetration depth} \tag{2.9}$$

Using the small cone penetrometer relative densities of the three samples prepared were estimated as 64%, 74% and 80% respectively, which agreed with another estimate made

by extracting carefully a sample of a known volume for the first two samples. In the first sample vibration was not applied, hence the lower value of relative density measured.

2.2.3 Water-saturated Redhill 110 sand

As for the oil-saturated sand, a filter at the bottom together with drainage and a fluid containment tank were set up to aid sample preparation (see Figure 2.13). The sand samples of 250 mm height were saturated by upward percolation of the water inside the tank of diameter 1100 mm and depth 400 mm. Once fully saturated, samples were then densified by vibration with a motor underneath the tank under a small confining stress. A surcharge of 1.5 kPa over a circular plate on top of the sample was used to assist the densification. Above the sand surface a column of water of approximately 130 mm was maintained.

To prepare a new sample the process was repeated with the only difference that the fluid in the containment tank was pressurised from the compressor line to create an upward flow which fluidised the sample, instead of gravity used for saturation. The vibration of the tank with the sample in it was halted once a target density was reached. The density was determined by measuring the weight and the volume of the sample.

2.2.4 Friction angle of the cohesionless soils

To obtain an effective peak angle of friction ϕ'_{peak}, Bolton (1986) proposed an expression that accounts for the density or packing of the sand by means of the relative density R_d, and also for the level of stress at failure, p'. The relative density is given as:

$$R_d = \frac{\gamma_{d\,max}}{\gamma_d}\frac{\gamma_d - \gamma_{d\,min}}{\gamma_{d\,max} - \gamma_{d\,min}} = \frac{\upsilon_{max} - \upsilon}{\upsilon_{max} - \upsilon_{min}} \tag{2.10}$$

either in terms of $\gamma_{d\,max}$, $\gamma_{d\,min}$ and γ_d (the maximum, minimum and current unit weights) or by using the maximum, minimum and current specific volume. The expression for the peak friction angle proposed by Bolton for plane strain and triaxial conditions respectively

is:

$$\phi'_{peak} - \phi'_{cs} = 5[R_d(Q - ln\, p') - 1]$$
$$\phi'_{peak} - \phi'_{cs} = 3[R_d(Q - ln\, p') - 1] \tag{2.11}$$

where p' is in kPa. Equation (2.11) is plotted in Figure 2.5 for the four sands used, where the solid curves correspond to triaxial strain and the dashed lines to plane strain conditions. Values of the effective angle of friction at critical state ϕ'_{cs}, for triaxial conditions are given in Table 2.1. In addition, values of $Q = 10$ and 8 have been used for silica and carbonate sand respectively. Dilatancy has its greatest effect at low mean effective stresses. However, when mean effective stresses reduce below 150 kPa no appreciable effect on soil behaviour occurs. On this ground Bolton (1986) suggests that stress level effects are not significant below $p' = 150$ kPa ($ln\, p' \approx 5$), then a compromise is to fix the value $ln\, p' = 5$ in Equation (2.11).

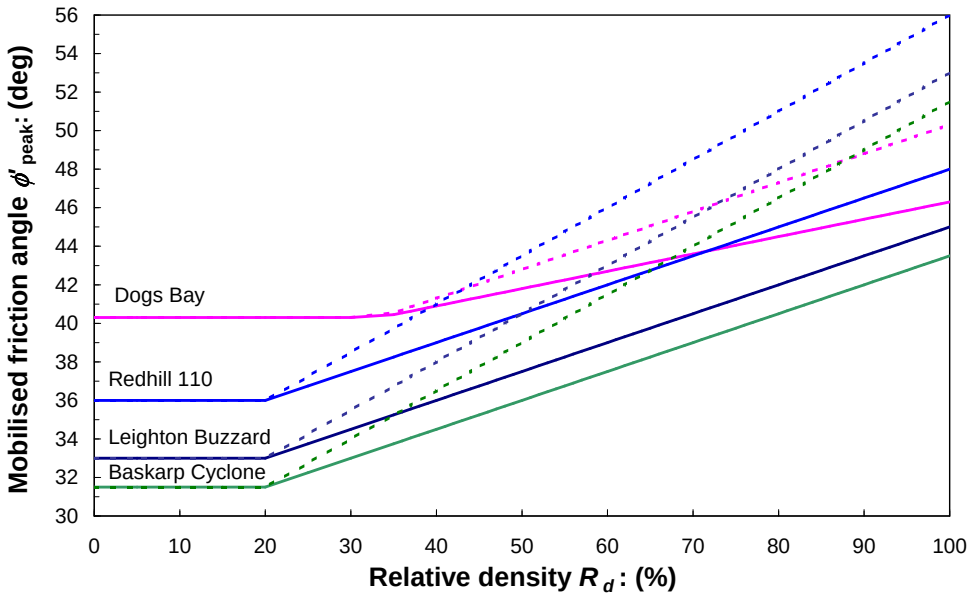

Figure 2.5: Variation of peak angles of shearing resistance ϕ'_{peak}, with relative density R_d, for the sands tested; solid curves for triaxial conditions and dashed curves for plane strain

2.2.5 Speswhite kaolin clay

The preparation of Speswhite kaolin clay specimens followed the method and procedures established since the one dimensional clay consolidation apparatus was designed and built by Gue (1984). This apparatus allows for the preparation of good quality homogeneous clay specimens with repeatable profiles of undrained shear strength and water

content with depth. Details of the design and operation of the apparatus are found in Gue (1984) and in de Santa Maria (1988). In preparing homogeneous kaolin slurry and subsequent consolidation of three specimens a similar sequence was followed to that described by Martin (1994). Briefly, a homogeneous material was obtained by mixing de-aired slurry at a moisture content of 120% in a ribbon blade mixer equipment with a vacuum pump. The slurry was pumped into cylindrical tanks of 450 mm diameter and 900 mm height. *Vyon* filters were then placed on top and the bottom of the specimens allowing drainage to atmospheric pressure during consolidation. Notwithstanding these similarities, a slightly different consolidation pressure path was applied, as can be observed in Figure 2.6. The

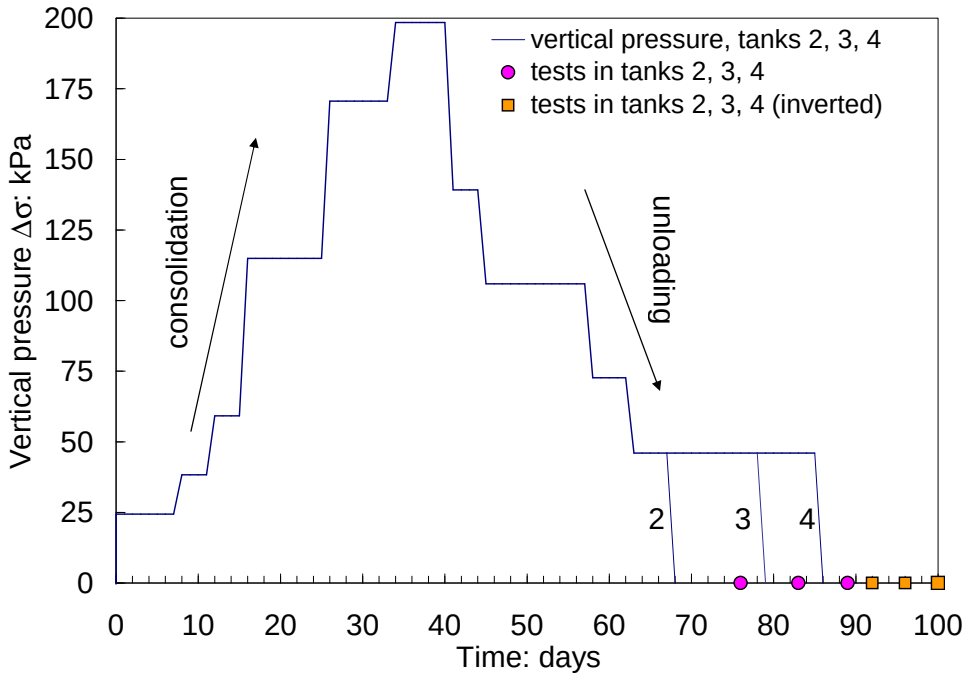

Figure 2.6: Speswhite kaolin clay consolidation and unloading pressures evolution with time for three tank (2, 3 and 4) showing in circles and squares the day of fully unloading and testing respectively

sequence of vertical pressure (25, 40, 60, 115, 170, 200, 140, 105, 70, 45, 0 kPa) allowed for a complete primary consolidation. The sequence of vertical consolidation pressures to reach 200 kPa took longer than the usual 3 or 4 weeks. At least 30 mm of space was allowed for filling with water the top of the sample. After fully unloading the sample a period of time elapsed to allow any negative pore water pressures developed in the swelling phase to dissipate. de Santa Maria (1988) carried out a "pushing up operation" allowing specimens to be extruded and cut after testing to remove the disturbed clay and

provide a second testing site. The square labels shown in Figure 2.6 represent a second series of tests carried out with the same specimens already prepared. However, these were not extruded and cut, but inverted and the undisturbed side of the specimens used instead.

The shear strength of each sample was measured using a shear vane apparatus shown in Figure 2.7(a). The apparatus is described by Bowden (1988) and subsequent modifications are described by Sills and Bartholomeeusen (2001). The vane diameter and length were $d = 12.65$ mm and $h = 30.3$ mm respectively (Figure 2.7(b)). The shear strength was calculated using the following equation:

$$s_u = \frac{T}{\frac{d^2 h}{2} + \frac{d^3}{2(n+3)}} \tag{2.12}$$

where the total torque $T = T_v + T_h$ is the contribution of the vertical and horizontal surfaces of the vane and is directly measured from the apparatus. The factor n was proposed by Wroth (1984) to include the effect of the shear stress distribution along the horizontal surface of the vane. Because of the lack of knowledge of an n value for the Speswhite kaolin clay, and to compensate for the friction along the extension rod and rate effects, it has been assumed equal to zero.

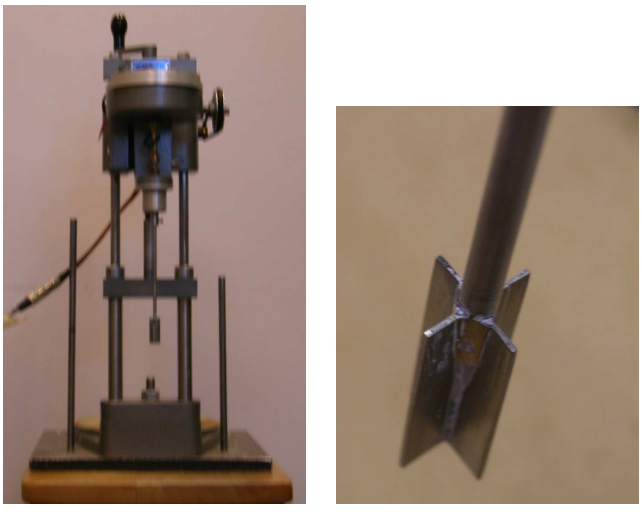

(a) (b)

Figure 2.7: (a) Shear vane testing device, and (b) vane

2.3 MODEL SCALE CAISSONS

The model caissons used are listed in Table 2.5 with a capital letter denomination. This denomination will be repeatedly encountered along the thesis, for brevity, when referring to caissons tested. The geometry and geometrical parameters also appear in Table 2.5. The length L and radius R or diameter $2R$, correspond to the *inside* skirt depth and to the *outside* diameter $2R$ respectively. Later on, to be specific, the radius will be referred as R_i, R_o or R to refer to the inside, outside or average radius. Caissons can also be classified by defining the aspect ratio $L/2R$ and the thickness ratio $t/2R$. Table 2.6 shows values of the caisson stiffness coefficients following the calculation procedure suggested by Doherty *et al.* (2005). The vertical, rotational, horizontal, and coupled stiffness coefficients K_V, K_M, K_H, and K_{MH} were calculated to assess the flexibility of the caissons compared with infinitely rigid caissons K_∞ and caissons without skirt K_0. In view of the results it is clear that the model caissons can be considered as practically infinitely rigid.

Table 2.5: Geometrical parameters of the model caissons tested

Caisson	A	B	C	D	E	F_{1-7}
Diameter, $2R$: mm	293	203.4	200	150	150	50.9
Length of skirt, L: mm	146.5	203.5	100	150	100	†
Thickness of the skirt wall, t: mm	3.4	3.4	1.0	1.0	1.0	1.66
Aspect ratio, $L/2R$	0.5	1.0	0.5	1.0	0.67	†
Thickness ratio, $t/2R$	0.012	0.017	0.005	0.007	0.007	0.033

†Caissons F

Caisson	F_1	F_2	F_3	F_4	F_5	F_6	F_7
L: mm	0	13.3	26	38.7	51	76.9	102.1
$L/2R$	0	0.26	0.51	0.76	1	1.51	2.01

Photos of the caissons are given in Figures 2.8(a), 2.8(b), 2.8(c), 2.8(d), and 2.8(e). The skirts of caissons F_{2-7} were fabricated from a brass tube, A and B from aluminium tubes and C, D and E from a corrosion resistant coper-aluminium alloy (duralumin or dural) plates. To account for the observation that, in general, a fine sand will mobilise more friction on a surface than a coarse sand, Uesugi and Kishida (1986) defined a normalised roughness $R_n = \frac{R_{max}}{D_{50}}$, where R_{max} is the maximum roughness (the height between the highest and lowest point of the surface profile). A smooth, intermediate and rough inter-

Table 2.6: Stiffness coefficients of the caissons ‡

Caisson	A	B	C	D	F_3	F_5
$K_{V\infty}$	10.26	16.47	10.26	16.47	10.26	16.47
K_V	10.25	16.43	10.24	16.38	10.26	16.44
K_{V0}	3.78	3.78	3.78	3.78	3.78	3.78
$K_{M\infty}$	16.70	68.44	16.70	68.44	16.70	68.44
K_M	16.54	67.17	16.39	65.58	16.62	67.74
K_{M0}	1.57	1.57	1.57	1.57	1.57	1.57
$K_{H\infty}$	9.81	17.18	9.81	17.18	9.81	17.18
K_H	9.74	16.89	9.66	16.58	9.78	17.01
K_{H0}	2.19	2.19	2.19	2.19	2.19	2.19
$K_{MH\infty}$	-7.69	-25.57	-7.69	-25.57	-7.69	-25.57
K_{MH}	-7.61	-25.14	-7.53	-24.55	-7.66	-25.35
K_{MH0}	-0.18	-0.18	-0.18	-0.18	-0.18	-0.18

‡assuming a caisson Young's modulus $E = 73$ GPa, sand shear modulus $G = G_R \left(\frac{z}{R}\right)^{\alpha}$, with $G_R = 1$ MPa and $\alpha = 0.5$

(a) Caissons F_{7-2}

(b) Caissons A and B

(c) Caisson A

(d) Caisson C

(e) Caisson D

Figure 2.8: Caisson models for dry sand samples: (a), (b); caissons for saturated soil samples showing the pore pressure transducer PPT and fluid valve: (c), (d), and (e)

face correspond to $R_n < 0.02$, $0.02 \leq R_n \leq 0.5$, and $R_n > 0.5$ respectively. Roughness was measured in the Metrology laboratory at the University of Oxford using a surface roughness machine (Taylor-Hobson Talysurf 4). A stylus tracks the surface profile through up and down movements which are followed by a strain gauged arm attached to it. From three measurements of roughness in different directions of the dural plate, R_{max} was con-

sidered to be in the order of 4 μm. Then, smooth interfaces result for Dogs Bay and Leighton Buzzard sands ($R_n = 0.017, 0.005$), whilst intermediate interfaces with Baskarp Cyclone and Redhill sands ($R_n = 0.07,\ 0.03$). Although, no roughness measurements were made for the brass and aluminium tubes, from tactile and visual observations of the surfaces and the sands used it is unlikely that a rough interface could occur.

Caissons A, C, D and E were equipped with air and fluid valves, and also with a pore pressure transducer PPT. A *Vyon* filter was located in the opening of the fluid valve to avoid particles passing through, with the risk of clogging the pipe, especially at the last stages of the suction installation. These features and the set-up of the suction system set-up are shown in Figure 2.13.

2.4 TESTING SITES AND BOUNDARY CONDITIONS

The boundary conditions chosen for the vertical loading tests included a fully filled cylindrical bed of dry Leighton Buzzard or Dogs Bay sand 1100 mm in diameter and 250 mm high. The F_{1-7} caissons were located symmetrically in nine sites as depicted in Figure 2.9. This minimises the variation in soil characteristics across different tests, which is particularly important when carrying out parametric studies. The most unfavourable condition occurs when the distance available between two caissons is 97 mm. Disturbance of the surrounding soil increases with the soil level of packing. Because of the local or punching shear failure mechanism developed in loose cohesionless soils the extension of the mobilised volume of soil is reduce to not more than a diameter. Even for a hypothetical general shear failure mechanism in loose sand, the disturbance can occur within two diameters for the longest caisson ($\frac{L}{2R} = 2$), assuming rough contact, $\phi' = 34°$, $\gamma_d = 15.7$ kN/m^3 and surcharge of 1.57 kPa (using ABC program by Martin, 2003). However, for dense samples the soil volume at failure might extend beyond the two diameters available. The ABC program (Martin, 2003) computes a plastic region that extends three times the

diameter of a rough circular footing, assuming $\phi' = 44°$, $\gamma_d = 17.2$ kN/m^3 and a surcharge of 1.72 kPa. It is important to bear in mind that the use of collapse mechanisms based on rigid plasticity and fully associated flow probably overestimates the distances. To overcome boundary effects tests were carried out leaving a site in between, and completing the series with the last half of sites which would suffer somewhat the effect of previously disturbed neighbour sites. However, for longer caissons the failure tends to not open widely to the surface, showing the transition to a deep failure mechanism.

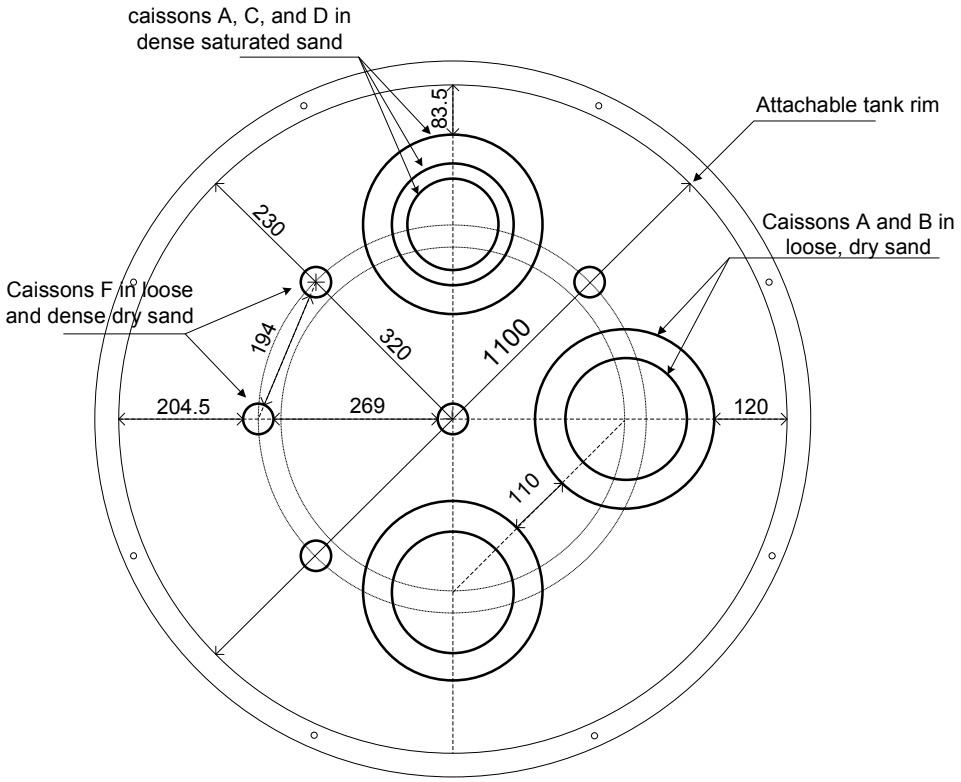

Figure 2.9: Plan view of the caisson's location inside the tank (dimensions in mm)

The use of caissons A and B for moment capacity tests constrains significantly the boundary conditions because of their larger size, as can be observed in Figure 2.9, in particular the distance to the bottom and wall of the tank is restricted. The former was solved by bolting on a ring of 150 mm thickness, as depicted in Figure 2.10(a), which increased the tank depth to 400 mm. The latter was mitigated incorporating spacers whose functions were to provide enough space between the ground surface and the loading apparatus to install these large caissons, and to switch the loading plane direction by 90°, so the caisson rotation acted on a larger volume of soil and not directly against the wall or towards the

centre, as seen in Figure 2.10(a). In principle, for a rotation or translation test in just one direction there would not have been interference, as long as a clockwise or anticlockwise sense is followed. However, for repetitive rotation tests interference between sites may occur. The maximum rotational displacement $2R\theta_{max}$ applied to the caissons is around 2 mm, inducing a maximum lateral displacement at the mudline level between $0.007L$ and $0.013L$ (caissons A and D). The disturbed extension at failure can be assessed in terms of the lateral earth pressure required to fully mobilise a wedge of soil. The disturbed extension at the ground surface is given by $L\tan(45° - \phi'/2)$ and $L\tan(45° + \phi'/2)$ according to the theoretical active and passive lateral earth pressure for smooth walls. The minimum lateral displacements of a rigid wall necessary to mobilise active and passive wedges are shown in Table 2.7. Bearing in mind that yield occurs previous to at least a fourth of $2R\theta_{max}$ (as it will be revealed in Chapters 5, 6 and 7), the lateral displacement rages between $0.002L$ and $0.003L$. Then, according to Table 2.7 passive wedges can not be fully developed, nevertheless, active wedges can develop particularly in dense sands. Therefore, it is expected that in clays and loose sands side boundary effects are negligible with a remote possibility of appearing far after yield has occurred, hence at the end of moment loading tests. Conversely, boundary effects can occur in the form of active wedges in dense sands. Furthermore, because a smooth and rigid-walled tank was used boundary effects are mitigated since lower earth pressures are generated in case of an active wedge reaches the tank. In the following chapters comparisons among test results will assess whether side boundary effects take place or not.

Table 2.7: Minimum lateral displacement to produce active and passive state (taken from Sowers, 1979)

Soil	Active state	Passive state
Dense cohesionless	$0.0005L$	$0.005L$
Loose cohesionless	$0.002L$	$0.01L$
Stiff cohesive	$0.01L$	$0.02L$
Soft cohesive	$0.02L$	$0.04L$

The clay specimens were approximately 420 mm height, so the water depth available was 30 mm. Only one caisson (caisson D) was tested in the centre of each side of the specimens prepared in tanks 450 mm diameter and 450 mm of height.

2.5 TESTING APPARATUS FOR MODEL FOOTINGS

2.5.1 The three-degree-of-freedom loading rig

To develop plasticity models is necessary to establish: (a) the yield surface, (b) the hardening law, (c) a flow rule, and (d) the elastic behaviour. Along the thesis these four components will be explored as part of hyperplasticity models. To develop a theoretical models the experimental study of foundation response requires a loading device capable of applying complex load or displacement paths. To this end a three-degree-of-freedom loading rig has been in operation at the University of Oxford since 1992. The rig was designed and built by Martin in 1992 to test model spudcan footings on an overconsolidated clay (Martin, 1994). Subsequently, Mangal (1999) and Byrne (2000) adapted the loading rig for applications of larger loads to test model footings on much stiffer soils. The rig, shown in Figure 2.10(a), can apply any planar combination of vertical, rotational and horizontal displacements $(w, 2R\theta, u)$ to a footing by means of computer-controlled stepper motors. Therefore, offshore environmental loads can be represented. In Figure 2.10(a) the numbers show: **1**, **2** and **3** the long LVDTs for vertical, horizontal and rotational displacements; **4**, **5** and **6** the stepper motors for vertical, horizontal, and rotational moves; **7** the waterproof shaft with the 'Cambridge' VMH load cell inside; **8** the circular base plate to attach the footing; **9** the model caisson footing; **10** the reaction frame; **11** soil sample; **12** tank; **13** spacers, and **14** I-beams.

Displacement controlled tests can be performed by means of independent control of three stepper motors, allowing the exploration of softening behaviour. The independent control over the displacements $(w, 2R\theta, u)$ is accomplished by using separate bearing and motion systems. The vertical and horizontal motion is provided by linear sliding plates, whilst the rotational motion is guided by a rotary sliding ring. The arm supporting the model footing is attached directly to the rotary sliding ring, allowing rotation of the footing without the need for a fixed centre of rotation. The stepper motors drive the plates and

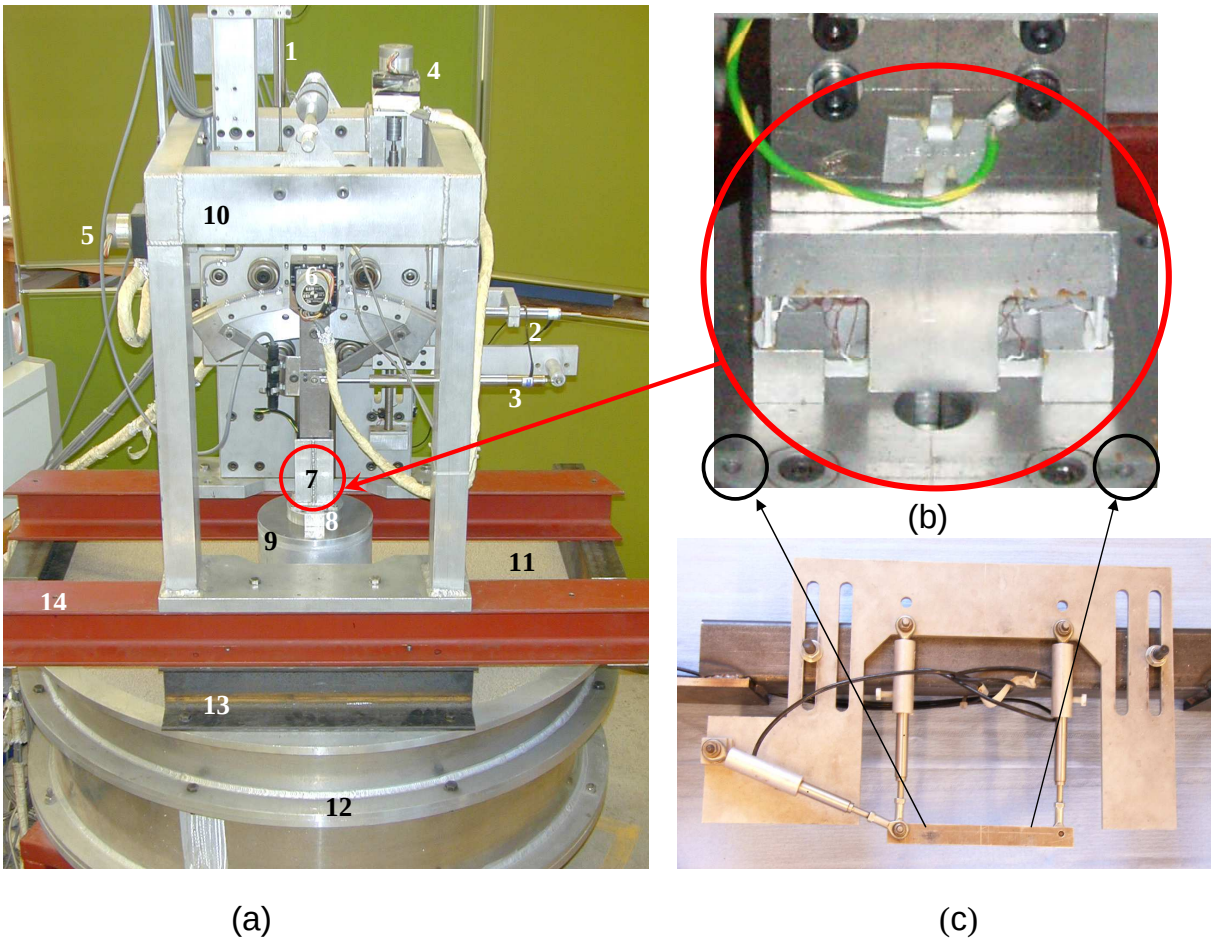

Figure 2.10: a) The three-degree-of-freedom VMH loading rig, (b) view of the 'Cambridge' VMH load cell, and (c) small LVDTs showing points of connection with base plate

ring with displacement ranges of $\Delta w = 300$ mm, $\Delta u = 50$ mm, and $\Delta\theta = 30°$. Figure 2.10(b) shows the "Cambridge" load cell (Bransby, 1973) attached to the rig arm and to the footing through a base plate allowing measurements of the resultant planar loads (V, M, H). The VMH load cell is composed of two aluminium blocks jointed by a system of strain-gauged webs, with the gauges connected into Wheatstone bridge circuits. There are four vertical and four horizontal webs forming two vertical circuits and one horizontal circuit. Each circuit is powered by 10 Volt DC supply and the resulting signal is amplified and translated to load units using a calibration constant. The load cell was already calibrated at the start of the testing programme and the matrix obtained from the calibration that relates the measurements of the strain gages with the loads was obtained by Byrne (2000). This matrix was incorporated within the acquisition program (Byrne, 2000) and used throughout the testing programme. The load cell was calibrated for a load reference

point (LRP) 10 mm below the centre of the base plate to which the footing is attached (LRP is discussed in section §2.5.3). The calibration involved the use of a calibration apparatus in which a load V, M or H is varied at the LRP whilst keeping the other two constant. The moment was applied by increasing the eccentricity of a constant vertical load. The horizontal load was applied by a wire passing through a pulley and connected to hanging weights. The vertical load is increased by hanging weights. Further information about the load cell calibration can be found in Martin (1994), Mangal (1999), and Byrne (2000). The load cell webs are restricted to a maximum strain ϵ of 0.001, giving a workable range of loads (without factor of safety) as shown in Figure 2.11. For example, for low vertical loads and for a horizontal load of 400 N, the maximum moment is around 50 Nm.

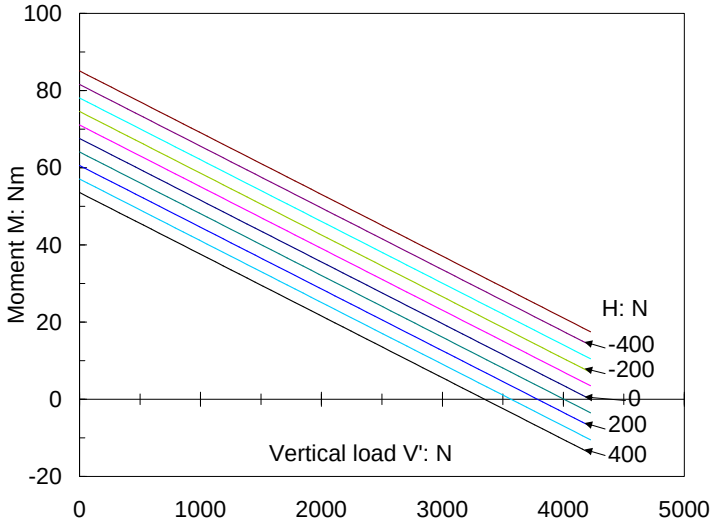

Figure 2.11: Load cell allowable loads (V', M, H) (Byrne, 2003)

To record footing displacements a system of three long range LVDTs was used. They were powered by a 5 Volts power supply and the resulting output signal was amplified and transformed to displacement units by means of calibration constants. As shown in Figure 2.10(a) the LVDTs follow the displacement of the sliding plates and the rotating arm of the loading rig from which the footing displacements can be deduced. This calculation is not strictly correct because the flexibility of the plates, ring, arm and any other component attached to the rig influences the real displacement of the footing. Therefore, correction due to rig flexibility is required. For the vertical loading tests presented

in Chapter 3, where $V_{max} \approx 500$ N, an additional LVDT measured directly the vertical displacement on the footing. Subsequent comparison of both recordings proved that differences were too small to represent a noticeable rig flexibility effect. Nevertheless, for combined loading tests when the moment is higher than 15 Nm and the horizontal load is higher than say 50 N, there is a need to account for the stiffness of the rig in the calculations of footing displacements. Thus, the footing displacements are corrected by adding to the long LVDT measurements the deformation suffered by the rig due to the loads, by means of a rig flexibility matrix [RFM].

$$\left\{ \begin{array}{c} w \\ 2R\theta \\ u \end{array} \right\}_{footing} = \left\{ \begin{array}{c} w \\ 2R\theta \\ u \end{array} \right\}_{rig} + [\text{RFM}] \left\{ \begin{array}{c} V' \\ M/2R \\ H \end{array} \right\} \tag{2.13}$$

Martin (1994) and Byrne (2000) determined this matrix for the rig. The cases of H less or larger than zero are treated separately. Adopting Byrne's matrix values,

$$[\text{RFM}] = \left\{ \begin{array}{ccc} -5.09 \cdot 10^{-4} & 8.31 \cdot 10^{-4} & -1.60 \cdot 10^{-4} \\ -1.07 \cdot 10^{-4} & 3.83 \cdot 10^{-3} & -2.06 \cdot 10^{-3} \\ 8.92 \cdot 10^{-6} & -1.81 \cdot 10^{-3} & 2.61 \cdot 10^{-4} \end{array} \right\} \quad \text{in mm/N for } H < 0$$

$$[\text{RFM}] = \left\{ \begin{array}{ccc} -5.09 \cdot 10^{-4} & 8.31 \cdot 10^{-4} & 1.70 \cdot 10^{-6} \\ -1.07 \cdot 10^{-4} & 3.83 \cdot 10^{-3} & -2.06 \cdot 10^{-3} \\ 8.92 \cdot 10^{-6} & -1.81 \cdot 10^{-3} & 2.49 \cdot 10^{-4} \end{array} \right\} \quad \text{in mm/N for } H > 0 \tag{2.14}$$

it is found that for any combinations of loads, where $V' > 500$ N, $M/2R > 50$ N, and $H > 50$ N, the corrections are of the order of 0.1 mm. Note that the two matrices in (2.14) differ only in the last column, which is associated with the horizontal load H.

Figure 2.10(c) shows a system of three short LVDTs designed by Byrne (2000) to obtain more refined displacement measurements. Although the short LVDTs offer a better resolution of the displacements $(w, 2R\theta, u)$, the stroke of each LVDT is limited to 10 mm. The small LVDTs were used mostly in cyclic tests where the long LVDTs provided a too

coarse resolution.

For footings in saturated soil, pore fluid pressure was measured using a PDCR 810 *Druck* pore pressure transducer PPT of ± 70 kPa range. The PPT was screwed to the top of the caisson lid and located in the plane of loading close to the caisson edge as shown in Figures 2.8(c), (d), and (e). A saturated *Vyon* filter protected the PPT strain-gauged diaphragm against direct contact with the soil.

The level of noise has a standard deviation for the loads of less than 0.5 N, for the long LVDTs between 6 μm and 30 μm, for the short LVDTs less than 2 μm, and for the PPT less than 50 Pa (Byrne, 2000). All displacements and loads were monitored and recorded using data-acquisition routines as well as being used within feedback control routines. All the electrical sensors were logged to a data-acquisition card located in a personal computer, with a maximum acquisition rate of 20 Hz. A MS Visual Basic 5.0 program written by Byrne (2000) allows the control of each of the three stepper motors independently. The control algorithm of a variable is a function of the *error* (between the current value and a specified value) and the *gain* to be determined to minimise the error. The gain depends strongly on the mean vertical load V_m, the range of loads (V', M, H), and the soil stiffness. Choosing appropriate values of the gain is very important for the appropriate implementation of the sequences of footing moves with or without V' or w *hold subroutines*; w hold subroutines are relevant for swipe tests, whereas V hold subroutine are relevant for moment loading tests at constant V'. A modified V' hold subroutine is relevant for suction installation tests, where the timer in the hold subroutine within the program is disabled. Any vertical load V' targeted, such as the scaled submerged weight of the structure, can be kept constant throughout the suction installation by carefully adjusting the suction applied to the interior compartment of the caisson.

More complex moves are required to generate a load controlled feedback subroutine, for instance to carry out cyclic loading tests. Byrne (2000) developed an algorithm able to read and reproduce an input file with a specified load history. The option of gain change

becomes available during the test, which can accelerate the displacement rate in case the targeted load is not been reached. A load control subroutine implemented for cyclic vertical loading tests is discussed further in section §7.2. More information about the loading rig can be found in Martin (1994), Mangal (1999), and Byrne (2000). No change or modification of the apparatus and of the MS Visual Basic 5.0 program was considered necessary to carry out during the testing programme.

2.5.2 The suction system

The suction needed to install a caisson in the field is usually developed by large capacity pumps such as submersible Remotely Operated Vehicles (ROV). Figure 2.12 shows a pump used for suction pile installations. A scaled pump could therefore be used for suc-

Figure 2.12: Suction pump unit on top of a suction pile (taken from SPT Offshore, http://www.suctionpile.com/pdf/SAPS001.pdf)

tion installations in the laboratory. The first attempt reported in a letter by Goodman *et al.* (1961) proved that small pumps were suitable to install "cups". Moreover, Wang *et al.* (1977) also used a pump and a small "medical aspirator" (peristaltic pump) for tests in clay. However, lately researchers have chosen other devices to generate suction such as those discussed at the ISOPE conference in 2001. There, House and Randolph (2001) and Kim *et al.* (2001) presented designs of computer controlled syringe pumps, which was implemented in centrifuges for the installation of suction caisson in clay and sand respectively. Using a suction pump and a depression vessel a suction percussive

technique was introduced by Allersma *et al.* (2001). The vessel is under suction through an crossover valve open to the pump. The valve is then close to the pump and open to the caisson compartment, applying instantaneously a large suction with short pulses. Once the pressure in the caisson and the vessel balances, the process is repeated until the caisson is fully penetrated. Allersma *et al.* (2001) pointed out that the main advantages of this technique over the gradual increase of the suction are: less likely to reach critical suction (piping), pump cavitation is avoided, and a better option to install caissons in layered soils and complicated seabeds is provided.

In the experimental work described here a simple and versatile water head difference method has been used. Sanham (2002) and Tran *et al.* (2004), among others, extensively used this method to study how different dead weights and flow rates affected the penetration under suction. The suction system developed is shown in Figure 2.13. Initially, tests were carried out to prove whether this method was suitable for a highly viscous fluid. This method was successful even for a caisson (not included in Table 2.5) with a thick skirt wall ($t = 3.4$ mm, and $R = L = 100$ mm), installed into a very dense oil-saturated Baskarp Cyclone sand sample ($R_d \approx 96\%$). Nonetheless, as calculations demonstrate, this caisson could be installed under a weight of $V' = 50$ N to achieve an initial self-weight penetration. Subsequent penetration was achieved under $V' = 50$ N by applying suction generated by a head difference. In particular, three variables were inspected, the reservoir pipe diameter (12.5 mm), a rough estimation of the head required (less than 400 mm) and the time necessary to install the caisson (between 1 and 4 hours).

A subsequent step was to connect a suction caisson to the VMH loading rig arm and to change the time subroutine within the control program, as explained in §2.5.1, to allow the suction installation of caissons. Once a suction caisson attached to the VMH loading rig was pushed into the ground between 15 to 30 mm with the bleed valve open (allowing the pressure inside the caisson to equilibrate with the pressure outside), the bleed valve was closed, and the fluid valve opened. Fluid in the caisson compartment was connected through a pipe to a reservoir, which was slowly lowered to increase the head difference h_f,

between the inside and outside of the caisson. The head difference could be increased to a maximum of 300 mm (3 kPa), whilst the vertical load applied to the footing was kept constant using feedback control.

For water-saturated Redhill sand samples the reservoir was connected to the suction caissons by a pipe with an internal diameter of 6 mm, instead of the 12.5 mm for the oil-saturated sand. The pipe length was chosen to allow sufficient water flow with minimal head loss. The valve connected to the water reservoir was much more sensitive to any change, therefore, it had to be open or close with more subtleness than for the tests in oil-saturated sand. This procedure allowed caissons to be installed by suction in sand

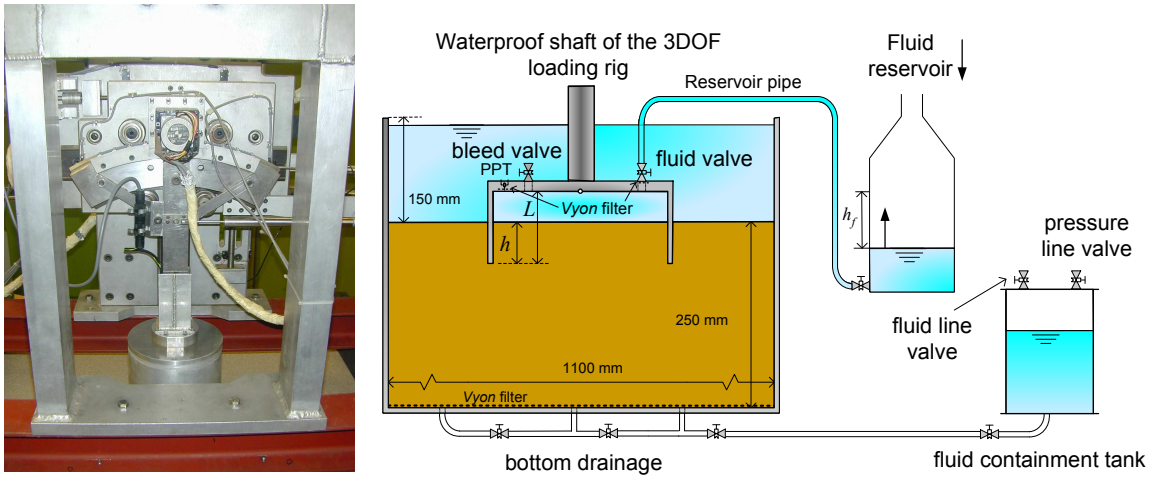

Figure 2.13: Diagram of the suction device

whilst connected to the loading rig. Once the suction phase was complete, it was possible to carry out combined loading tests similar to those carried out on the dry sand.

For installations in clay the suction was applied by using a vacuum pump, as previously reported by Rauch *et al.* (2003) for suction piles ($L/2R = 9$). The 1 atm vacuum line was connected to a system of containers and valves before to be attached to the caisson. The system ensured that no fluid could pass through to the vacuum line system and also allowed the operator to regulate and control the suction applied.

2.5.3 The reference point for loads and displacements

An idealised sequence of the installation is shown in Figure 2.14. It is an idealisation since it does not consider any rearrangement or remoulding of the soil surrounding the skirt caused by the caisson penetration. From the sequence in Figure 2.14 the convention

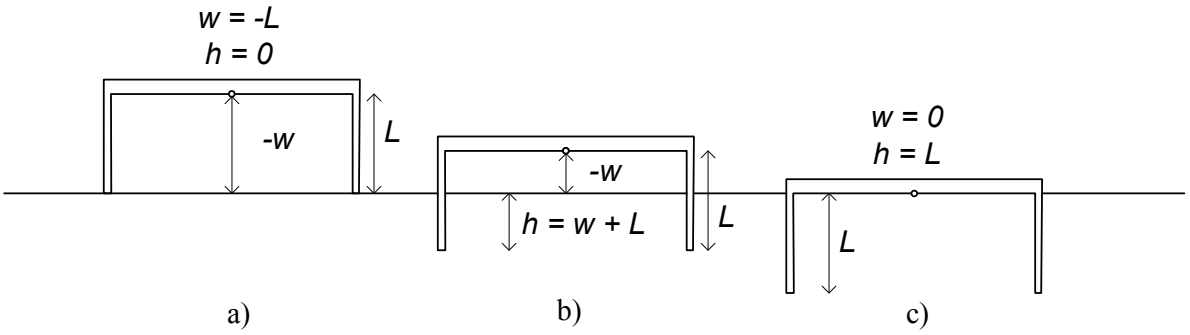

Figure 2.14: The vertical displacement during a caisson penetration in terms of w and h: (a) initial installation, (b) semi installed, and (c) fully installed

for caisson penetration is h and settlement is w once the caisson is installed, whilst vertical displacement will be generic, *i.e.* either h or w.

For loads and displacements the convention given by Butterfield *et al.* (1997) is assumed. Figure 2.15(a) illustrates this convention adopted for a fully installed suction caisson, where the combination of vertical, moment and horizontal loads $(V', M/2R, H)$ is associated with the respective set of vertical, rotational and horizontal displacements $(w, 2R\theta, u)$. Careful consideration must be given to the load reference point, particularly if it is different to that defined in Figure 2.15(a). Figure 2.15(b) illustrates the case of loads located by a structural engineer, for instance at a distance d above that according to Butterfield *et al.* (1997) or Figure 2.15(a). Although neither V' nor H modify their magnitudes or directions, for equivalent loads attention must be paid to the change in magnitude of the moment M, which becomes:

$$M' = M + d\,(H\cos\theta + V'\sin\theta) \tag{2.15}$$

where d is the distance between the load-application point and the load reference point chosen. Furthermore, as illustrated in Figure 2.15(c), the rotation θ in both positions is the same, but the horizontal displacement u, as well as the vertical displacement w,

undergo the following modifications:

$$\begin{aligned} u' &= u - d\sin\theta \\ w' &= w + d\cos\theta \end{aligned} \tag{2.16}$$

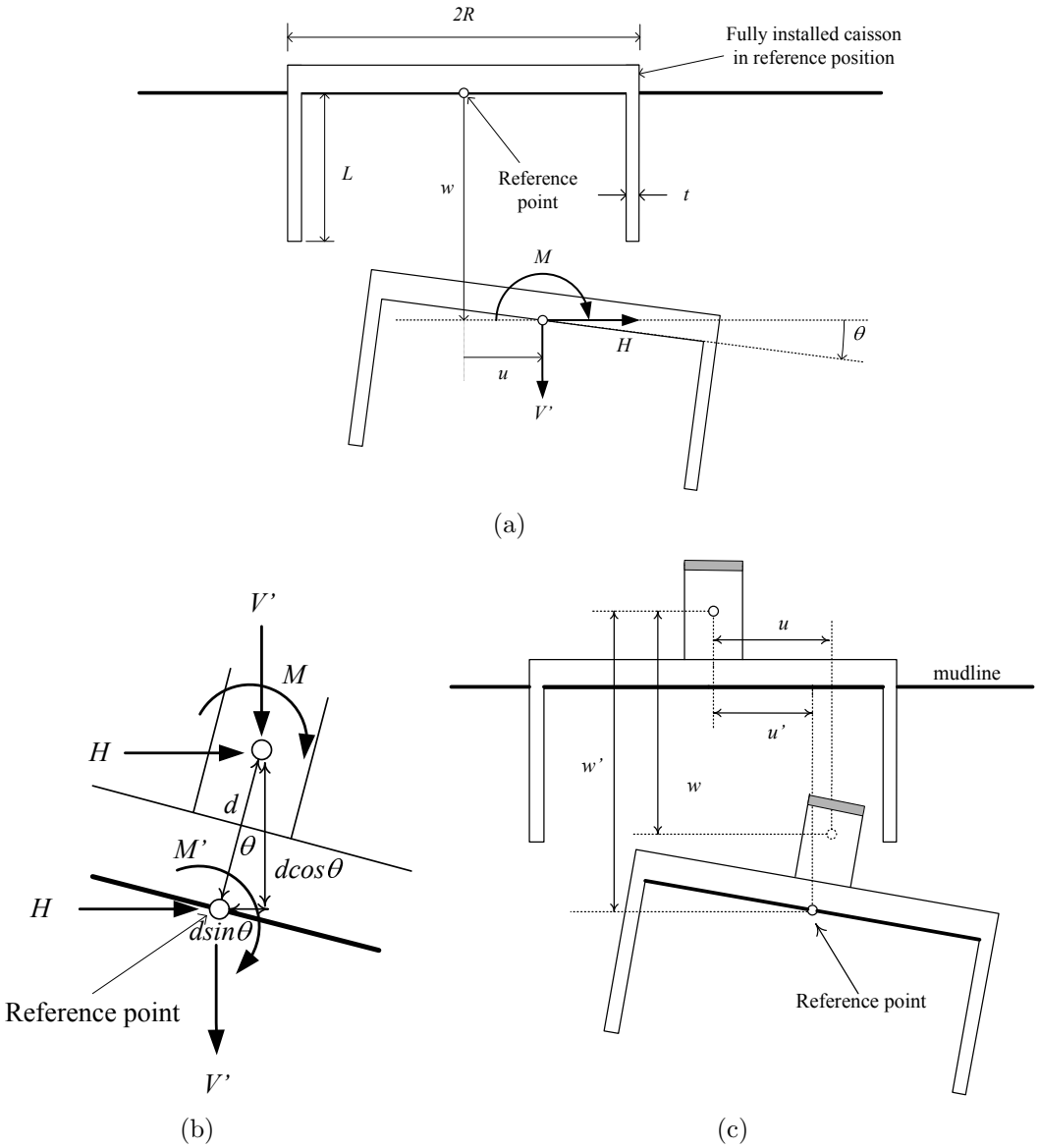

Figure 2.15: Coordinate system employed showing: (a) load and displacement components for a VMH combining loading, (b) loads applied to a certain point and the equivalent loads transfered to the reference point, and (c) displacements occurring in a certain point and the equivalent displacements transfered to the reference point